

MASTER'S THESIS 2018

**Stability performance indices in an AC
network with VSC-HVDC and a large
share of non-synchronous generation**

ISAK HELLGREN AND JOHANNA TRILLKOTT



CHALMERS
UNIVERSITY OF TECHNOLOGY

Department of Electrical Engineering
Division of Electric Power Engineering
CHALMERS UNIVERSITY OF TECHNOLOGY
Gothenburg, Sweden 2018

Stability performance indices in an AC network with VSC-HVDC and
a large share of non-synchronous generation
ISAK HELLGREN AND JOHANNA TRILLKOTT

© ISAK HELLGREN AND JOHANNA TRILLKOTT, 2018.

Supervisors: Peiyuan Chen, Department of Electrical Engineering
Frank Johansson, ABB HVDC System Technology
Erik Kilander, ABB HVDC System Technology
Magnus Öhrström, ABB HVDC System Technology

Examiner: Massimo Bongiorno, Department of Electrical Engineering

Master's Thesis 2018
Department of Electrical Engineering
Division of Electric Power Engineering
Chalmers University of Technology
SE-412 96 Gothenburg
Telephone +46 31 772 1000

Cover: Equivalent network representation of a North American utility with two
VSC-HVDC stations presented in detail in Appendix A.

Typeset in L^AT_EX
Printed by Chalmers University of Technology
Gothenburg, Sweden 2018

Stability performance indices in an AC network with VSC-HVDC and
a large share of non-synchronous generation
ISAK HELLGREN AND JOHANNA TRILLKOTT
Department of Electrical Engineering
Chalmers University of Technology

Abstract

With the increased penetration of non-synchronous generation from renewable energy sources worldwide, more research on how to describe and evaluate the stability of any given network is needed. In this master thesis, the objective is to define and investigate key performance indicators (KPIs) for assessing how and to what extent VSC-HVDC systems may be used for increasing the stability margin in weak AC networks with a large share of non-synchronous generation. To define suitable KPIs for this purpose, thorough studies of relevant literature have been made and followed up by simulations on two different power systems in PSS[®]E. The first of these two is a classical 4-machine system designed by Prabha Kundur, while the second is a more realistic network based on an islanded utility in North America.

From the studies, two KPIs for describing short-term frequency stability are selected; the frequency nadir, i.e. the lowest frequency the power system experiences after a disturbance, and the rate of change of frequency (ROCOF) directly after the perturbation. Further on, the short circuit capacity at different buses in the system is selected as a KPI for evaluating the voltage stability of the power network in case of large disturbances. For voltage stability related to small disturbances, the dV/dQ , describing the incremental change of AC voltage in response to changes in load reactive power, is suggested as a KPI. The studies also show that the short circuit capacity alone can no longer be used for describing the voltage system strength of any network, and to address this, dV/dQ is proposed as a complement.

Finally, the simulations in PSS[®]E show that VSC-HVDC using fast frequency response can improve the frequency nadir and the ROCOF of a power system during disturbances in generation. The voltage control of the VSC-HVDC may also improve the dV/dQ of buses close to the HVDC terminal more than an equivalently sized synchronous generator. Thus, VSC-HVDC can contribute to the frequency stability and the voltage stability related to small disturbances of any power system.

Keywords: Power system stability, virtual inertia, fast frequency response, VSC-HVDC, short circuit capacity, frequency nadir, rate of change of frequency, dV/dQ , voltage stability factor

Acknowledgements

Our work on this master thesis started in January 2018, and was completed in the beginning of June the same year. Research was undertaken at the Department of Electrical Engineering at Chalmers University of Technology and at the ABB HVDC facility in Ludvika, Sweden. Over the past five months, we had the great privilege of many rewarding discussions with our supervisors at ABB and Chalmers.

First of all, we would like to thank Erik Kilander, Frank Johansson and Magnus Öhrström at ABB HVDC System Technology in Ludvika for valuable feedback and support throughout the semester. Thank you for giving us the opportunity to perform this master thesis.

A great thanks to Peiyuan Chen for showing interest in our work and contributing to the thesis with helpful discussions and guidance, especially regarding power system stability and on how to discuss our simulation results.

We would also like to express our gratitude to Massimo Bongiorno for giving us tools for critically evaluating our results and conclusions, improving the academic level of our work.

Finally, we would like to thank Niklas Modig at Svenska Kraftnät for answering our questions on how the Swedish TSO works with frequency stability, now and for the future.

Isak Hellgren and Johanna Trillkott, Gothenburg, June 2018

Contents

Abbreviations	i
Parameters	ii
1 Introduction	1
1.1 Background	1
1.2 Aim	2
1.3 Renewable energy and AC system strength	2
1.3.1 Definition of weak AC systems	4
1.4 Method	4
1.5 Scope	5
2 Power system stability	9
2.1 Basic concepts and definitions	10
2.1.1 A simple power system representation	10
2.1.2 Kinetic energy and inertia	11
2.1.3 Swing equation	11
2.1.4 Short circuit capacity	12
2.2 Frequency stability	13
2.2.1 Power balance and system frequency	13
2.2.2 Frequency control	14
2.2.3 System response to a large disturbance	14
2.3 Voltage stability	16
2.3.1 Small-disturbance voltage stability	16
2.3.2 Large-disturbance voltage stability	17
3 HVDC technology	19
3.1 An introduction to HVDC	19
3.2 Motivation for VSC-HVDC in weak networks	19
3.3 Basic operation of VSC-HVDC	20
3.3.1 Control strategies	22
3.3.2 Limitations in active and reactive power	23
4 Key performance indicators	25
4.1 Frequency stability parameters	25
4.1.1 Rate of change of frequency	25
4.1.2 Frequency nadir	26

4.1.3	Time to nadir	27
4.1.4	Inertia	27
4.1.5	Primary frequency response	28
4.2	Selection of frequency KPIs	29
4.2.1	Simulation studies in MATLAB Simulink	30
4.2.2	Final selection	33
4.3	Voltage stability parameters	33
4.3.1	Short circuit capacity	33
4.3.2	dV/dQ	34
4.4	Selection of voltage KPIs	36
4.4.1	PSS [®] E simulations on a basic power system	37
4.4.2	Final selection	38
5	Simulations on Kundur's network	41
5.1	Introduction to the Kundur network	41
5.2	Evaluation of frequency KPIs	42
5.2.1	Summary	44
5.3	Evaluation of voltage KPIs	45
5.3.1	Summary	47
6	A more realistic simulation case	49
6.1	Introduction to the network	49
6.2	Evaluation of frequency KPIs	49
6.2.1	Summary	54
6.3	Evaluation of voltage KPIs	54
6.3.1	Summary	56
7	Discussion	57
8	Conclusion and future work	59
	References	61
A	Simulation models and networks	I
A.1	Hydro governor model in Simulink	I
A.2	VSC-HVDC model for PSS [®] E simulations	I
A.3	The Kundur network	II
A.4	The more realistic network	IV
B	Dynamic measuring methods	IX
B.1	Measuring dV/dQ dynamically in PSS [®] E	IX
B.2	Measuring SCC dynamically in PSS [®] E	X

Abbreviations

AGC	Automatic generation control
EV	Electric vehicle
HVDC	High-voltage direct current
IGBT	Insulated-gate bipolar transistor
KPI	Key performance indicator
LCC	Line-commutated converter
MMC	Modular multilevel converter
PFR	Primary frequency reserve
PLL	Phase-locked loop
PSS [®] E	Power system simulator for engineers
p.u.	Per unit
TSO	Transmission system operator
TOV	Temporary overvoltage
VSC	Voltage-source converter
VSF	Voltage stability factor

Parameters

Parameter	Unit	Description
dV/dQ	-	Voltage deviation in per unit to a change in load reactive power in per unit
FFR	MW	Fast frequency response
f_{nadir}	Hz	Lowest point of frequency after a disturbance
H	s	Inertia constant
ROCOF	Hz/s	Rate of change of frequency directly after a disturbance
SCC	MVA	Short circuit capacity
t_{nadir}	s	Time between the disturbance and the f_{nadir}

1

Introduction

The power transmission systems of today consist traditionally of large, centralised power plants and passive networks with unidirectional power flow from the generation units to the loads. Fossil energy resources such as coal, oil and natural gas are still commonly used for power generation in most parts of the world, even though they have proved to cause severe damage on the climate due to the emission of greenhouse gases such as CO_2 . At the same time, the global electricity demand is predicted to increase significantly in a near future.

A way to reduce greenhouse gas emissions in power systems is by introducing a larger share of renewable power sources such as wind and solar generation to the grid. However, as non-synchronous generation replaces traditional synchronous generation, the stability of the power network is affected as less rotating mass is present in the grid. This reduces the robustness of the system and may cause a loss of stability in the network. The loss of stability can be counteracted by different measures for power system stability support, such as synchronous condensers supplying reactive power or power electronic converters regulating active and reactive power using advanced control systems. An example of the second option is high-voltage direct current (HVDC) systems with voltage-source converters (VSC) that are commonly used for connecting asynchronous grids and offshore wind farms.

1.1 Background

One of the leading companies worldwide in HVDC and other electrification products is ABB [1]. Over the last decade, along with the rapid growth of renewable energy sources, ABB has had an increase in enquiries of HVDC converters using the VSC technology. When designing HVDC connections, ABB receives different requests from grid owners on how VSC-HVDC can or should behave during faults in the system, among others. However, more research on how VSC-HVDC interacts and adds functionality to conventional AC networks, by for example contributing to the stability of the power system, is needed. In addition, another main issue is that per today there is a need for defining common parameters to describe the functionality that VSC-HVDC could contribute with simplifying the communication

between the manufacturers of HVDC, grid owners and experts in the field. Thus, there is an increasing need to investigate measures for evaluating and comparing the functionality of VSC-HVDC converters with traditional stability functions in the power grid.

This thesis is written with support from ABB, and with the main objective to map and define parameters needed to describe system stability in weak AC systems with a large share of non-synchronous generation and VSC-HVDC. This work is highly relevant not only for electrification companies such as ABB but for any grid owner globally, as it is of great importance to take the stability of the power system into account when integrating new components into the grid. To efficiently and safely operate a power grid, the transmission system operator (TSO) needs to set reasonable requirements for companies supplying power generated by non-synchronous power plants. However, in most countries worldwide it is still rare to find any formal requirements in for example grid codes for the functionalities related to power system stability support that could be provided by non-synchronous generation sources. This could be explained by that there is a technology shift in the power system field per today, and that the TSOs thereby are unsure of which technical requirements to demand to ensure stable power system operation in systems including for example large wind farms and HVDC links connected to the system using power electronic converters. Thus, by mapping parameters needed to describe a power system including VSC-HVDC and formulating suitable requirements for these parameters, this thesis work is beneficial for TSOs when formulating grid codes.

1.2 Aim

The objective of this master thesis is to investigate and define key performance indicators (KPIs) to assess how and to what extent VSC-HVDC can improve stability margins in a weak AC network with a large amount of non-synchronous power generation.

1.3 Renewable energy and AC system strength

With the rapid increase of non-synchronous power sources connected to the grid using power electronic converters, new challenges such as reduced system inertia are introduced to the power systems. To give an idea on how fundamental this change is globally, examples from the TSOs in Sweden, UK and the US are given in this section. The choice of these three countries is due to that they are facing different challenges related to the shift into more non-synchronous generation in the power grids. Lastly, a definition of what makes an AC system weak is presented, to illustrate the relation between non-synchronous generation and AC system strength.

Swedish scenario

According to Svenska Kraftnät's system development plan, released in November 2017, the goal is that the power generation in Sweden should consist of 100% renewables in 2040 [2]. By this time, the Swedish nuclear reactors are expected to have shut down and the corresponding power production will be covered up by a significant increase of wind power. Solar PV on rooftops are also expected to increase to about 7 TWh yearly over the same time frame. The Swedish population is expected to increase by 18% until 2040, with a larger need for electricity as an effect. However, the energy efficiency will also improve, and the total increase in power usage is expected to increase from 140 TWh today to 150 TWh in 2040 [2]. More information about this can be found in [2].

UK scenario

In the report Future Energy Scenarios released by National Grid in 2017 and found in [3], it is stated that new nuclear reactors will have to be built in a near future for decreasing the CO_2 emissions from the electricity generation, along with a large increase in capacity by renewable power sources, mainly offshore wind power [3]. Energy storage is presented as a vital part of the future British power system, as the power generation from coal is to be replaced by other generation sources before 2025. Until 2050, the electricity demand is expected to increase as natural gas, which today is supplying most of the energy usage in the UK, is exchanged for electricity. The peak power demand is predicted to increase with up to 2% annually over the same time frame with the higher electricity demand and due to the increased use of electric vehicles (EVs) [3].

US scenario

In [4], the National Renewable Energy Laboratory (NREL) states that the US has abundant and diverse sources of renewable energy. Thus, the deployment of renewable energy sources is expected to increase significantly in the future, from 10% in 2010 to about 80% in 2050. In specific, about 50% of the power generation in 2050 is expected to come from wind power and solar technologies. To enable such a large share of variable power sources, grid storage and flexibility of load are essential. According to the Energy Information Administration (EIA), the annual growth in electricity demand is predicted to about 1% until 2050, even though efforts are made to increase the power usage efficiency [5]. However, it is difficult to predict the future power demand in the US as it is largely dependent on the electrification of the transport sector. If EVs get a significant breakthrough, the electricity demand may increase considerably [6].

Challenges for the power systems

In summary, the amount of non-synchronous power generation and EVs are expected to increase significantly in all three countries until 2050. However, this results in different challenges for the three countries, as their power systems are fundamentally different. In the UK, the challenges are mainly connected to the decreased system

inertia, as the UK is an island nation without synchronous connection to power systems in continental Europe [3],[7]. The US, on the other hand, has an extremely large power system and thus the inertia is not of large concern. Instead, other factors such as having sufficient power reserves in all parts of the system at all time needs to be ensured [8],[7]. Sweden has both sufficient inertia and power reserves in the grid per today. Still, as nuclear power units are shutting down in Sweden, there is a need for investigating how this will affect the stability of the Nordic power system and how to formulate requirements on the new generation in grid codes [2],[9].

1.3.1 Definition of weak AC systems

One question of great concern is how the system strength of AC systems worldwide will be affected by this shift of technology in the power grids. According to *IEEE guide for planning DC links terminating at AC locations having low short circuit capacities*, found in [10], an AC system including HVDC can be defined as weak based on two different aspects:

- The equivalent impedance of the AC system is high relative to the DC power at the point of connection, or
- the inertia of the AC system is inadequate in relation to the DC power infeed.

The equivalent impedance of an AC system is closely related to the short circuit capacity (SCC) of the network, defined in section 2.1.4 [10]. As non-synchronous generators do not naturally contribute with short circuit current during faults, the SCC decreases when the share of non-synchronous generation in the system increases. At the same time, as the non-synchronous generators do not automatically contribute with inertial response to the system either, the inertia constant of the system, as defined in section 2.1.2.1, will decrease. This issue is discussed more in detail in section 4.1.4. Overall, the power system strength by this definition will inevitably reduce as a larger share of the electricity comes from non-synchronous power sources.

1.4 Method

The thesis work began with a literature study of scientific papers, books and conference proceedings on power system stability and HVDC found using Chalmers' library database Summon. The literature was then complemented by information on HVDC systems provided by ABB. An investigation of TSO reports on power system stability and future challenges of their networks was also performed. The focus for the TSO reports has been on the Nordic, Irish, UK and North American transmission system operators. This is due to the high penetrations or projections of non-synchronous generation in these power systems, which has prompted more

research into the stability of modern networks. These countries were also chosen as the challenges in these networks are of different nature, as discussed in section 1.3, which has given this thesis a more general outlook. The information from the TSO reports were confirmed by an interview with Niklas Modig at the Swedish TSO Svenska Kraftnät.

Based on the literature study, KPIs were chosen for further research using simulation studies in MATLAB Simulink and PSS[®]E. In a first stage, the simulations were performed on small and basic networks, resulting in a selection of KPIs that appeared to have the ability of correctly describing the frequency and voltage stability of power systems with a large penetration of non-synchronous generation and HVDC. Next step was to evaluate the usability of the KPIs using simulation studies in PSS[®]E on two different power system models: a 4-machine network designed by Prabha Kundur and a larger and more realistic network based on a North American utility.

Kundur's network is a classical network with only synchronous generation. Thus, simulations were firstly made to assess the selected KPIs and to verify that the KPIs are applicable for assessing power system stability. Then, a generator was replaced with an HVDC station and the KPIs were assessed once more to investigate the usefulness of the KPIs when power electronic converters are present in the grid. These two test cases with and without HVDC also demonstrates the impact of the VSC-HVDC on the system stability compared to an equivalently sized synchronous generator.

Finally, the simulation studies on the more realistic network were performed to validate that the KPIs are useful in a more practical system, and to quantify the changes in system stability that are caused by VSC-HVDC. These simulations were also made to further investigate how the KPIs can be used to describe system strength in a network with non-synchronous generation and VSC-HVDC.

1.5 Scope

As presented in chapter 2, power system stability may be classified into three different types: frequency, voltage and rotor angle stability [11]. These types of stability have different effects on the power system depending on the time frame and the size of the disturbance. The emphasis in this report will be on short-term frequency and voltage stability. This is mainly due to that these are the areas where TSOs globally see future stability problems related to the increased portion of renewables in the systems, as indicated in for example [4], [7] and [9]. In addition, the selected KPIs should be suitable for describing the strength of any power system, and it should be possible to affect the KPIs using VSC-HVDC. As the stability contribution of the VSC-HVDC is mainly connected to its ability to rapidly change its power output and the direction of the active and reactive power flow to the system, the time frame of interest for the KPIs is short-term.

Even though several different models to represent VSC-HVDC exist, only one HVDC model will be used in the PSS[®]E simulation studies for this project. This is related to that the aim of the project is not to design the most stable solution for any specific case, but to assess the overall characteristics of the VSC-HVDC and its impact on selected KPIs in weak AC systems. The selected VSC-HVDC model is an HVDC Light base model developed and commonly used by ABB. The model is equipped with a main circuit design based on ABB HVDC Light standard module configuration M9, found in [12]. This model is a typical VSC-HVDC model that ABB promotes, and is assumed to provide the basic characteristics of VSC-HVDC connections used globally. For the HVDC model, vector control is used in all test cases, as this is the most common control system for VSC-HVDC per today.

When investigating the functionality of VSC-HVDC regarding its ability to contribute to the frequency stability of any network, fast frequency response (FFR) provided by the HVDC converters is applied. In section 4.1.4.1, FFR is introduced together with virtual inertia, which are stability support functions that can be provided by power electronic converters. However, the focus in this report is on FFR, as this is a method commonly used in literature for simulating the effect of a fast acting active power support from power electronic converters during frequency contingency events [13], [14]. Thus, the HVDC converters are not controlled to mimic inertial response, which is the case when providing virtual inertia.

Further on, no non-synchronous generators such as wind power models are implemented in the test systems. This is due to that a wind turbine, which is the most common type of non-synchronous generator per today, is connected to the power system using converters in a similar way as VSC-HVDC. Thus, the results from simulation studies made on HVDC converters will also be valid for converters connecting wind farms to the grid. Further on, large wind farms are often connected to AC systems using HVDC links, and is thereby never directly connected to the synchronous system. Thus, the HVDC connections in the test systems are considered to be the connections of non-synchronous generation to the synchronous networks.

In the simulation studies of the basic network in PSS[®]E as well as the Kundur network where the functions of the VSC-HVDC model is compared to the characteristics of a conventional generator, only one type of generator will be considered. This generator is a standard salient generator model with an exciter and a governor, and is commonly used to represent hydro turbines in PSS[®]E. This choice has been made as hydro turbines are common synchronous generators in the Nordic as well as in European and American power systems, and they are expected to be continuously used in the future as hydro power is a highly reliable source of emission free and clean electric power. When comparing simulation cases with only generators with HVDC cases, the same load conditions are used, and the load models are as basic as possible to simplify the comparisons.

For the power system case study based on the North American utility, more than one VSC-HVDC model is connected to the network. In this case, the interactions between the two VSC-HVDC models are not investigated. This could be of interest

for future work focusing on how to maintain the stability of a weak power system over time, but will not be assessed in this thesis as it has no impact on which KPIs that should be assessed when evaluating the system stability.

Finally, when suitable KPIs are selected, not much effort is spent on trying to optimise the use of these parameters for any specific case. Instead, the main idea is to give a broad overview of which parameters that should be considered for AC systems with VSC-HVDC, and how these parameters relates to each other and to the operation of VSC-HVDC converters.

2

Power system stability

The stability of any system is generally defined as the ability to remain in a state of operating equilibrium under normal operating conditions and to regain this state after being exposed to a physical disturbance. This fundamental definition is also used for power system stability [15]. The stability of a power system has traditionally been a concern of the behaviour of synchronous machines, where operating equilibrium is said to be obtained when these machines are kept in synchronism. However, power system instability may be encountered without loss of synchronism, such as when the system is subjected to a voltage collapse [15]. In addition, for the power system to remain in operating equilibrium, the power flows in the network must settle at reasonable values. From these factors, three types of power system stability can be defined, namely rotor angle stability, voltage stability and frequency stability. These three types of stability can be categorised further depending on the size of the disturbance and the time span, as indicated in Figure 2.1 [11].

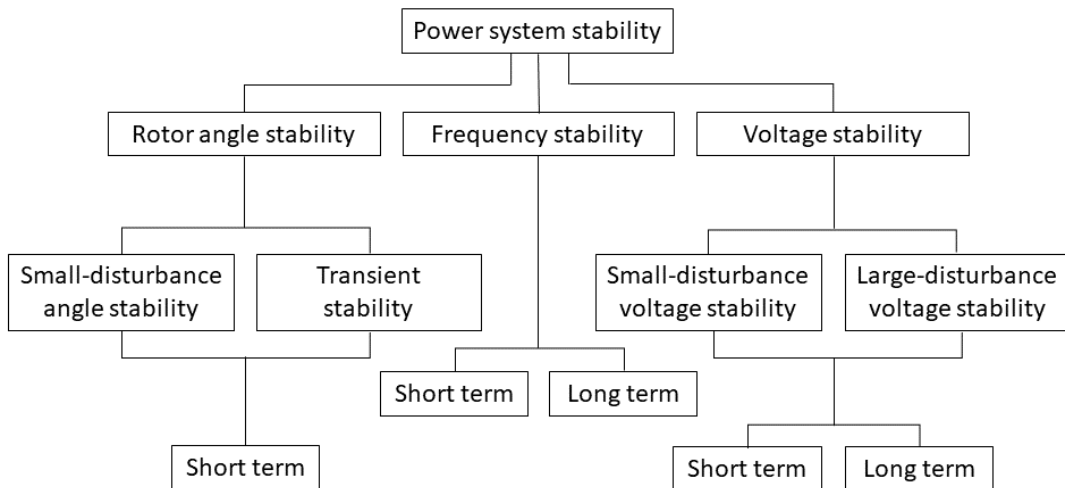


Figure 2.1: Classification of power system stability depending on the physical nature of the stability problem, size of the disturbance and the time span [11].

Further on, small disturbances are connected to small perturbations that continuously occur in power systems and that may be linearised around their operating points [16]. Large disturbances, on the other hand, are connected to larger pertur-

bations, such as loss of a line or a large machine. Generally, the generating units and protective devices in a power system should be dimensioned to ensure that the system can handle loss of its single largest unit, i.e. the dimensioning fault. When this is the case, the power system is said to be (N-1) contingent.

In this chapter, the fundamentals of power system stability are described, defining basic concepts such as kinetic energy, inertia, the swing equation and short circuit capacity. Then, frequency and voltage stability are explained more in detail.

2.1 Basic concepts and definitions

This section defines central concepts of power system stability, beginning with a simple representation of a power system. The rotational energy of a synchronous machine is related to the inertia constant, and this relation is extended to power systems with several interconnected machines. Then, the swing equation is introduced and related to the inertial response provided by a synchronous machine. Finally, the concept of short circuit capacity of an AC system is explained.

2.1.1 A simple power system representation

A basic schematic representation of a power system consists of generating units, loads and a transmission system. In a traditional power system, the generating units are synchronous machines generating active power which is supplied to the loads through transmission lines that are mainly inductive, in accordance with Figure 2.2. The unidirectional power flow in such a simple power system can be expressed as

$$P = \frac{V_1 V_2}{X} \sin \theta, \quad (2.1)$$

where V_1 and V_2 are the voltage magnitudes at the point of connection of the generator and load respectively, X is the line reactance and θ is the transmission angle, i.e. the angle difference between the generator and the load.

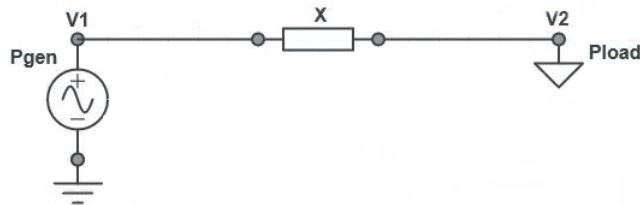


Figure 2.2: A simple power system representation with a generator producing active power P_{gen} and a load consuming active power P_{load} , connected by a transmission line with inductive impedance X .

2.1.2 Kinetic energy and inertia

From fundamental physics, kinetic energy can be expressed as

$$E_{kin} = \frac{m \times v^2}{2}, \quad (2.2)$$

where m is equal to the mass of a system and v to the velocity in m/s. This expression can be used to describe the kinetic energy of a rotating machine by transferring it to the rotational frame, translating it into

$$E_{rot} = \frac{J \times \omega_r^2}{2} \quad (2.3)$$

where J is the moment of inertia of the rotor and ω_r is the angular velocity expressed in rad/s. The rotational energy E_{rot} is measured in Ws, and is commonly referred to as the “inertia” of the system, and is defined as the resistance to a change in state of motion. Thus, the inertia is basically the energy stored in the rotating mass of a synchronous machine which will oppose any change in kinetic energy in the system.

2.1.2.1 The inertia constant

The inertia constant H , also referred to as the inertia time constant, is defined as the stored rotational energy E_{rot} at synchronous speed divided by the machine rating S in MVA [15]. It is expressed in seconds and calculated as

$$H = \frac{E_{rot}}{S} = \frac{J \times \omega_r^2}{2S}. \quad (2.4)$$

H can be interpreted as a measure of the time a synchronous machine can output rated power before the speed of the rotor is reduced to zero [17]. The relation in (2.4) can be expanded for a system with many synchronously connected machines, where the aggregated inertia constant H_{sys} can be calculated as

$$H_{sys} = \frac{\sum_{i=1}^n (S_i \times H_i)}{S_{tot}}. \quad (2.5)$$

In (2.5), n is the number of synchronous generators connected to the system, S_i is rated power of generator i and H_i is the inertia constant of the i th generator [14], [18]. S_{tot} is the total rated power of the system expressed in MVA.

2.1.3 Swing equation

One of the most central equations describing the stability of a power system is the swing equation, presented in (2.6) [15]. The swing equation gives a relationship

between the rotational mass of a synchronous machine and the mechanical and electrical torques acting on the rotor of the machine [15].

$$J \times \frac{d\omega}{dt} + D \times \omega = T_m - T_e \quad (2.6)$$

In this equation, D is a damping constant accounting for the windage and friction losses of the synchronous machine, T_m is the mechanical torque and T_e is the electrical torque. When the T_m is equal to T_e , there is no net torque acting on the rotor, and thus there is no acceleration in the system [15]. However, when the machine is subjected to a disturbance, a net torque is applied to the rotor and thus the rotational speed changes. This change in speed will be affected by the system inertia, and thus the swing equation describes the motion of the machine. Further on, using the definition of the inertia constant H given in (2.4), the swing equation can be expanded as

$$\frac{2HS}{\omega_r^2} \times \frac{d\omega}{dt} = T_m - T_e \quad (2.7)$$

$$\frac{2H}{\omega_r} \times \frac{d\omega}{dt} = P_m - P_e, \quad (2.8)$$

where P_m and P_e are the mechanical power input from the turbine and the electrical output in p.u. respectively [19]. In these equations, the damping has been neglected.

2.1.4 Short circuit capacity

Short circuit capacity can be defined in different ways depending on if the SCC is to be calculated for a synchronous machine or for an AC system as seen from a specific node. In this report, SCC is one of the measures used for characterising the strength of an AC system and is calculated as the product of the three-phase fault current I_{SC} and rated pre-fault voltage V at the bus of interest, as expressed in (2.9)[20].

$$SCC = \sqrt{3} \times V \times I_{SC} = \frac{V^2}{Z_{th}} \quad (2.9)$$

SCC is most commonly expressed in MVA. When calculating the SCC, it is assumed that the AC system can be represented by a Thevenin equivalent voltage source behind a Thevenin equivalent impedance Z_{th} at fundamental frequency [10]. Thus, SCC is proportional to the inverse of the Thevenin equivalent impedance of the system, as shown in (2.9). In a classical system with mainly synchronous generation, a high SCC indicates a strong system with stiff voltages, i.e. the voltages do not deviate largely from their initial values after a disturbance. On the contrary, a low SCC indicates a weak system with voltages that deviates far from their original values when subjected to large disturbances.

2.2 Frequency stability

Frequency stability can be defined as the ability of a power system to return to its initial value of frequency, or another acceptable steady-state operation point, within a finite time after being exposed to a disturbance [11]. The power system frequency, in turn, reflects the balance between the supply and demand of power, as the system frequency is kept constant as long as the generation and load are balanced [19]. Thus, every power system is designed for a certain frequency, and the system frequency must lie within a predefined range not deviating too far from the frequency the system was designed [14]. For the Nordic power systems, and most other power systems around the world except North America, the nominal system frequency is 50 Hz. To ensure high power quality, the allowed range of deviation from this value is $\pm 0.2\%$ [17]. However, the Nordic power system is able to handle frequency deviations of about ± 1 Hz without collapsing.

To maintain the system frequency within safe boundaries, frequency control functions are used. If the frequency deviates too far from its nominal value, protective devices are activated to protect the system components and to keep the power system operational [21]. In this section, the fundamentals of frequency stability are described, and then an introduction to frequency control is given.

2.2.1 Power balance and system frequency

In every power system and at each instant of time, the supply and demand of electric power must be equal for the system to remain in a state of operating equilibrium. In section 2.1.3, the swing equation gives a relationship between the rotational mass of a synchronous machine and the power balance between the mechanical input power of the turbine and the electrical power output. This relation can be expanded to cover a system of several interconnected synchronous machines, where all machines works together to supply the system loads while keeping the rotational speed, and thus the system frequency, constant. To illustrate how the system frequency changes with the angular velocity of the synchronous machines, the swing equation presented in (2.8) can be rewritten as

$$\frac{df}{dt} = \frac{f_0 \Delta P}{2H_{sys} S_{sys}}. \quad (2.10)$$

In (2.10), df/dt is the change in frequency the system experiences after a disturbance, f_0 is the nominal frequency and ΔP is the difference between P_{gen} and P_{load} [22]. From this equation it can be seen how the rotational speed is affected by disturbances in power balance, or vice versa [15]. It also shows that the inertia of the system dictates how fast the frequency changes in response to a disturbance.

2.2.2 Frequency control

As discussed in the beginning of this chapter, a power system is generally considered stable if it is (N-1) contingent. This refers to that the system should be able to continue its normal operation when the single largest component is disconnected. When a large generator trips, the frequency control will react and stabilise the power system frequency within seconds, restoring it to nominal value within 15 minutes [14]. Then, the power system frequency is controlled by adjusting the output of the other generators connected to the system to compensate for the sudden loss of generation. In this section, the two actions of providing this kind of frequency support, known as primary and secondary frequency control, are described.

2.2.2.1 Primary frequency control

Primary frequency control is the action of generators to rapidly and autonomously change their power output to oppose a change in system frequency [8]. The primary frequency control should be able to respond within a few seconds, preventing the frequency to transcend the allowed range of frequency deviation and to arrest the frequency decline at an acceptable value. For a generator to be able to contribute to the primary frequency control, it must be on-line and having a head room, i.e. a difference between the current operating point and its maximum operating capability [8]. The primary frequency control includes governor response, which is provided by most traditional generators such as hydro and thermal turbines. However, primary frequency control is usually not provided by nuclear generators and wind turbines.

2.2.2.2 Secondary frequency control

In contrast to primary frequency control, secondary frequency control is a centrally directed action to change the power output of interconnected generators in the system. Secondary frequency control is thereby provided more slowly than primary frequency control, and reacts after tens of seconds to minutes. Secondary frequency control can be either manual or automatic, using automatic generation control (AGC), and aims to restore the system frequency to its nominal value [8].

2.2.3 System response to a large disturbance

The behaviour of the system frequency after a large disturbance is illustrated in Figure 2.3. In the figure, it can be observed that the frequency decline after the disturbance is arrested by a combination of system inertial response and primary frequency control. Then, the primary frequency control stabilises the system frequency at a constant value above the lowest allowed frequency limit of the power system [8].

Within 15 minutes, secondary frequency control is provided to the system, restoring the frequency to its nominal value [14].

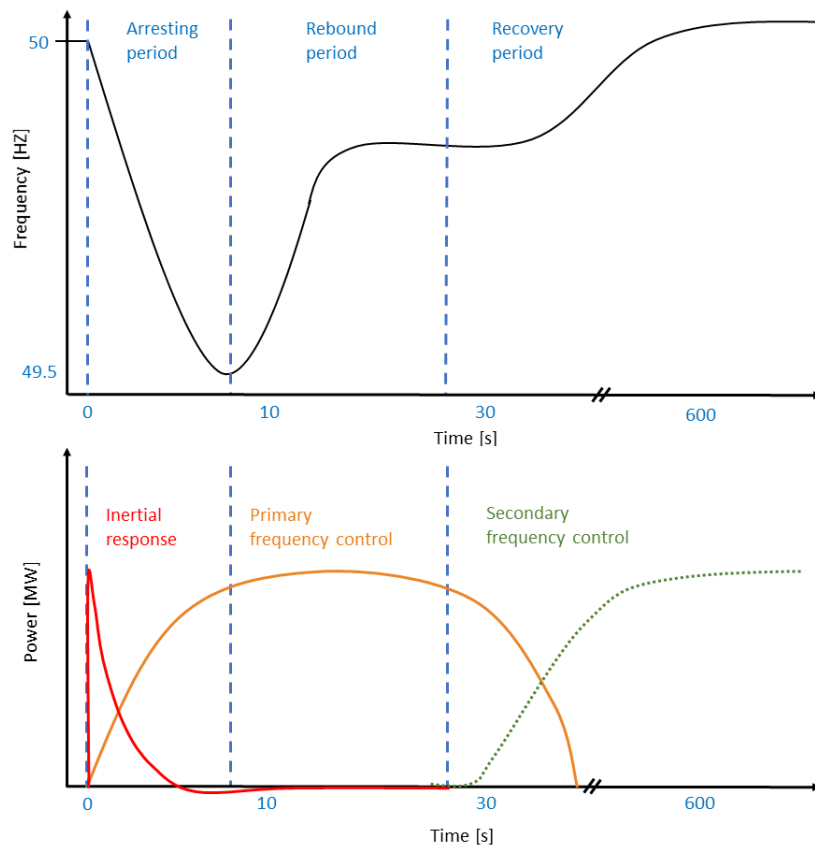


Figure 2.3: In the upper picture, the change in system frequency following a disconnection of a large generator is illustrated. The frequency decline is arrested by the inertial response of the system and by the use of primary frequency control, shown in the picture below. Then, the frequency is restored to its nominal value using secondary frequency control [8].

If the frequency of a power system is declining very rapidly after a large disturbance, closing in to the lowest allowed frequency limit, it is common that safety control systems of the network starts to disconnect loads, i.e. begins load shedding. This generally occurs at predetermined load shedding levels above the lowest under-frequency limit and is used as a last resort to avoid a total system collapse. However, in most networks worldwide, load shedding is avoided as much as possible and is therefore a rare event.

Finally, worth to notice is that in this report, a disturbance is generally described as a case where the power balance is disturbed such that the load exceeds the generation, which happens when a generation unit is disconnected from the system while the demand is kept constant. Then, the system frequency starts to decline, as shown in the figure. Still, the opposite action, where load is suddenly disconnected and the generation exceeds the demand, is also possible. However, as it is significantly easier to handle such events only by reducing the power output of generators connected to

the system, this is generally not seen as a challenge for the network stability and is therefore not considered in this report.

2.3 Voltage stability

Voltage stability can be defined as the ability of a power system to maintain steady voltages at all buses in the system after having been subjected to a disturbance [11]. The most common driving force for voltage instability is load dynamics, as the loads try to draw more reactive power than what can be delivered after a disturbance. A power system that is not voltage stable may undergo a voltage collapse when it is subjected to a large disturbance. This refers to that the voltage decreases below acceptable limits and may cause a partial or a total power system blackout [20].

In this section, the two overall types of voltage stability will be investigated: voltage stability after small disturbances and after large disturbances, from now on referred to as small-disturbance and large-disturbance voltage stability.

2.3.1 Small-disturbance voltage stability

As briefly mentioned in the introduction to this chapter, small-disturbance voltage stability is related to small perturbations in voltage where the power system may still be linearised around its operating point [16]. Small disturbances occur continuously in a power system when loads are connected and disconnected, and thus, this type of voltage stability is also referred to as steady-state voltage stability [20], [23]. Small-disturbance voltage stability is commonly analysed using P-V and Q-V curves. These methods are used to determine the loadability limits related to the voltage stability, and are calculated using power flow simulation programs [20]. In Figure 2.4, P-V curves for different load power factors are shown. One way of extending a P-V curve and thus the loadability margin, which is the distance on the x-axis from the active operating point to the maximum power point, is to supply the system with more reactive power.

In Figure 2.4, it can be seen that for a given load power P below the maximum power point, also known as the nose-point, there are two possible voltage solutions for each P . One solution is located at the upper part of the curve, and the second solution is found on the lower part, as indicated by the intersections of the black solid line and the dashed line in the figure. The upper voltage solution is the accepted solution, as this one has a voltage magnitude within the allowed range of 1 ± 0.05 p.u. This solution is also the stable one since an increase in reactive power at this operating point increases the voltage magnitude. On the contrary, continuous operation on the lower solution is not acceptable since in such a case an increase in reactive power would reduce the voltage [16]. This is an unstable behaviour as a voltage control system usually measure voltage and increases Q when the voltage is lower than the

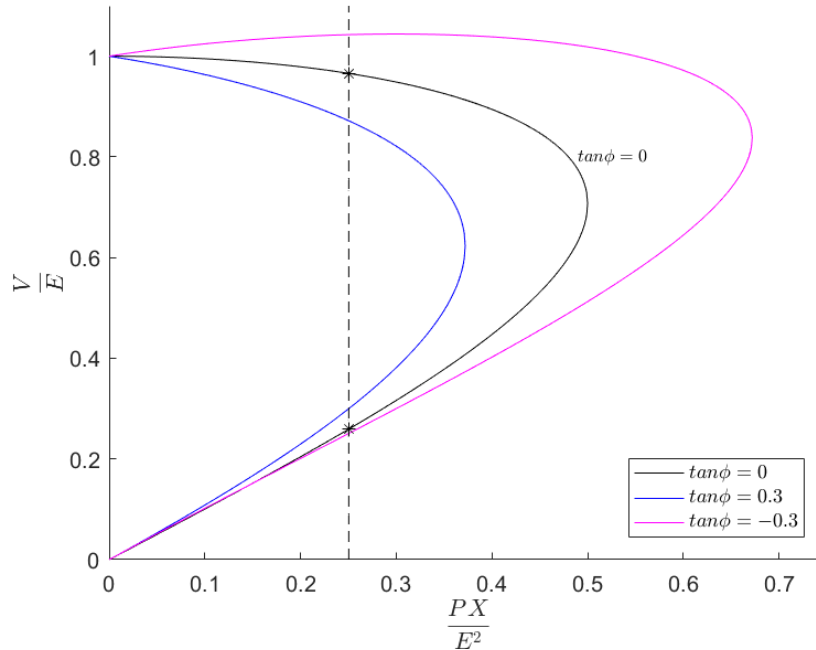


Figure 2.4: P-V curves for different load power factors, $\tan \phi$ [16]. The x-axis is normalised load power P with respect to short circuit power, E^2/X , and the y-axis is normalised load voltage V with respect to sending end bus voltage E .

reference value. For the lower operating point, the low voltage would trigger the control system to increase Q , which in turn would reduce the voltage even further. Thus, the voltage would continue to fall until the system collapses.

2.3.2 Large-disturbance voltage stability

A power system is said to be large-disturbance stable if it reaches an acceptable steady-state operating point within finite time following a large disturbance [10]. The large-disturbance voltage stability, also known as transient voltage stability, of a power system is generally classified using SCC, presented in section 2.1.4. This type of voltage stability is closely connected to the strength of the network, as the bus voltages in a power system with high SCC relative to system load is more likely to recover, and to recover faster, after a large perturbation than in a power system with low SCC.

3

HVDC technology

Today, HVDC links are used globally for interconnecting asynchronous power grids or connecting remote islands and offshore wind farms to the mainland. In this chapter, the HVDC technology with emphasis on VSC-HVDC is presented and explained, as that is the type of HVDC converter used in this report. Firstly, a short introduction to HVDC is given, and then motivations to why VSC-HVDC is preferred over LCC-HVDC in weak AC systems are presented. The basic operation of VSC-HVDC converters are described, and finally control strategies used for VSC-HVDC converters are presented.

3.1 An introduction to HVDC

The idea of using HVDC for power transmission over long distances is not new. In 1954, the first commercial submarine HVDC cable, developed by ASEA, was connected between Ygne, Gotland, and Västervik at the Swedish mainland [12]. The early HVDC installations used mercury-arc technology. However, line-commutated converter (LCC) HVDC using thyristors was soon introduced, and is still today the most common type of HVDC installations worldwide [12]. Mercury-arc HVDC and LCC-HVDC both rely on the stiffness of the AC voltage to operate [24]. This fact motivated the invention of the next HVDC technology, using voltage-source converters, which was first introduced in 1997 by ABB under the name of HVDC Light [12], [25]. VSC-HVDC is fundamentally different from the LCC technology as it uses insulated-gate bipolar transistors (IGBTs) instead of thyristors, allowing for other types of converter topologies. The VSC-HVDC has also the ability to produce its own voltage without support from the network [24], in contrast to LCC-HVDC.

3.2 Motivation for VSC-HVDC in weak networks

Depending on situation it is sometimes preferable to use VSC-HVDC over LCC-HVDC, and vice versa. LCC-HVDC has lower transmission losses and are thus preferred for large installations interconnecting strong grids [12]. However, when

connecting to weak AC systems, it is beneficial to use VSC-HVDC. There are mainly three factors to this. The first one is that LCC-HVDC consumes reactive power up to 60% of the rated power of the LCC-HVDC for commutation of the thyristors. Therefore, large capacitor banks are needed to supply reactive power. The capacitors can cause temporary overvoltages (TOVs), where the magnitude of the TOVs are increased when the SCC is decreased [24]. The maximum power transfer of the LCC-HVDC is also limited by the SCC, and thus, the strength of the AC network highly impacts the operation of the LCC-HVDC [24], [25].

Secondly, another issue with LCC-HVDC in low SCC networks is that the capacitors and filters needed for operation produces harmonic content and specifically low-order harmonic resonances. The VSC-HVDC does not have these issues as it does not need capacitors to supply reactive power nor filters due to its multilevel converter setup, discussed in section 3.3 [24], [25].

The last factor to why VSC-HVDC is preferred over LCC-HVDC in weak AC grids is that the VSC-HVDC can, in contrast to the LCC-HVDC, separately control how much active and reactive power to output. The voltage-source converters at each end of the VSC-HVDC link can also output reactive power independently of the other. This enables a variety of functionalities of the VSC technology in weak networks, as it can rapidly change the output reactive power in response to disturbances to increase the overall dynamic performance of the AC network [26]. The independent reactive power control also results in that there is no lower limit on the SCC for the VSC-HVDC to continue its operation, as the VSC-HVDC does not need any support from the network to commutate its valves.

In summary, VSC-HVDC solves many of the issues with the LCC technology in low SCC networks and facilitates for operation of HVDC in networks of any strength, as classified by SCC in section 1.3.1 [25]. VSC-HVDC can also provide additional services to weak AC networks such as voltage stability support due to its fast, independent active and reactive power controls [27], [28].

3.3 Basic operation of VSC-HVDC

The basic operation of a VSC-HVDC system involves converter topology and control of the IGBTs to correctly output the reference voltage and current. In addition, control schemes for determining voltage and power references based on factors such as network conditions and operator input are of importance, as described in 3.3.1. Lastly, the limitations in active and reactive power of the HVDC converter are discussed in section 3.3.2.

There exists many realisations of VSC-HVDC where IGBTs are used in different configurations. The realisation that is in focus in this section is the modular multilevel converter (MMC), which is the basis for today's HVDC Light technology [12] used in this report. The MMC topology uses modules consisting of two valves,

which include an IGBT and a diode each, and a capacitor connected in parallel to the valves, as seen within the black dashed boxes in Figure 3.1. The modules are connected together in series along with phase reactors, L , and a transformer. In the figure, U_V is the valve voltage and U_L is the network AC voltage. Figure 3.1 represents one phase of the HVDC station. Any number of modules can be used in an HVDC station, but with increasing number of modules, less harmonic content is produced as the output waveform more closely resembles the reference sinusoidal waveform. However, at the same time the complexity increases in valve control, and module failures are more probable with more components connected in series.

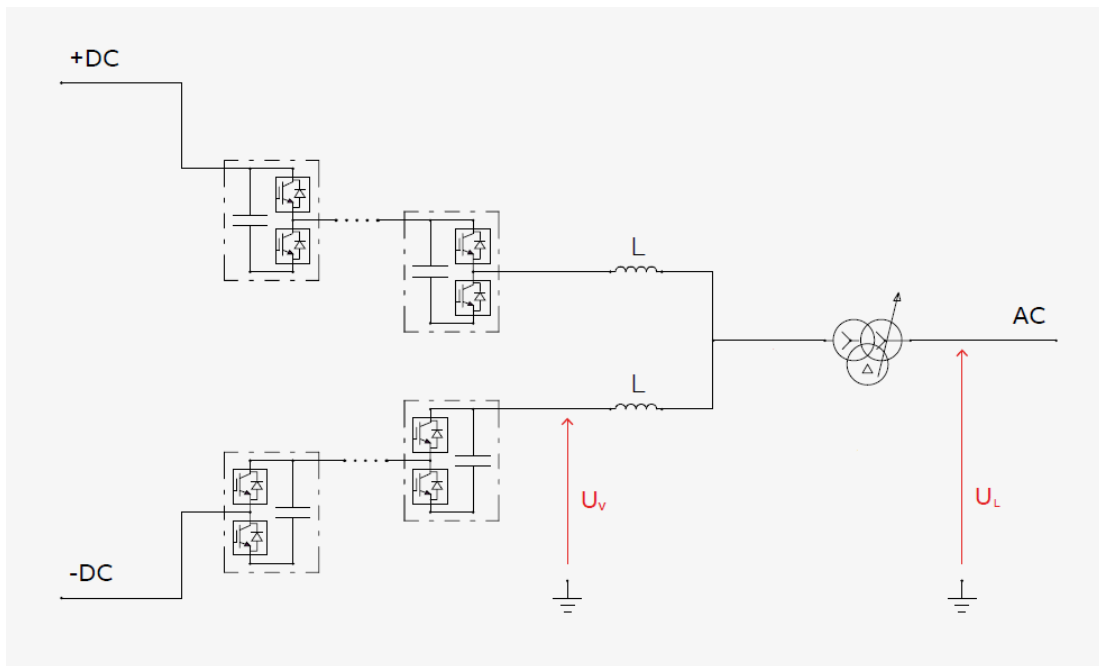


Figure 3.1: Schematic representation of one phase of the multilevel VSC with IGBT modules, phase reactors L and a transformer. U_V is the valve voltage and U_L is the network AC voltage [12]. Photo courtesy of ABB.

In order to produce sinusoidal AC voltage, the IGBT valves are switched in a certain sequence. For example, if the bottom valve in one of the modules shown as dashed boxes in Figure 3.1 is switched on, the capacitor is connected in series and increases the voltage. In contrast, if the top valve is switched on, the capacitor is bypassed and thus the module does not increase the voltage. The choice of how many modules that contributes to shape the voltage changes the number of distinct levels in the voltage waveform that the converter outputs. When the converter changes from a few to all modules contributing to the voltage, one module at a time, the voltage steps up. The reversed action is used to step down the voltage. This way of stepping up and down the voltage is used to produce the voltage waveform seen in Figure 3.2, which displays a waveform produced by a five-level multilevel converter. In the figure, the blue line marks the reference voltage.

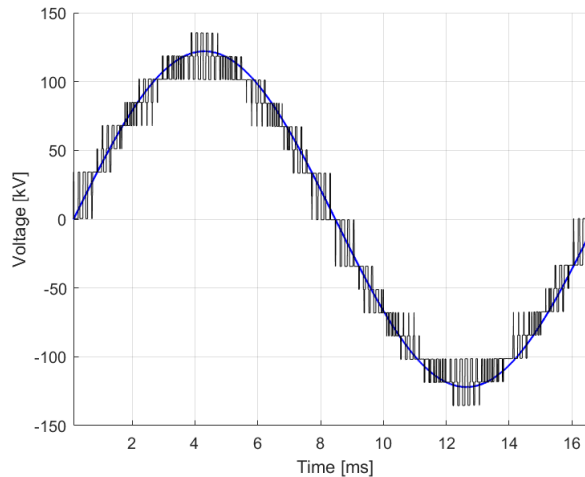


Figure 3.2: An example of a reference voltage (in blue) and an output voltage (in black) produced by a five-level multilevel converter [24].

3.3.1 Control strategies

The basic idea of VSC-HVDC control systems is to regulate the valve voltage U_V to a specific amplitude and phase such that the converter outputs scheduled active and reactive power. This is achieved by measuring U_L and controlling the current through the phase reactor, L , to achieve the correct U_V voltage [12]. In Figure 3.3, the basic control structure for VSC-HVDC is given. In the middle of the figure the AC current control block is located with outer voltage, reactive power, active power and DC voltage control blocks. It can also be seen that the operator has the choice of selecting active power or DC voltage control as well as AC voltage or reactive power control. Of the two HVDC stations on each end of the HVDC link, one HVDC station has to be in active power control and the other set to DC voltage control in order to maintain stable transmission. However, the choice of AC voltage or reactive power control can be selected independently for both stations [27].

When designing the control blocks shown in Figure 3.3, there are many different designs and control philosophies, as discussed in detail in [24]. In the case of VSC-HVDC, the usual practice is to decouple active and reactive parts of the current by transforming the current into the dq-reference frame. Thus, one can control the active and reactive power independently. A phase-locked loop (PLL) is used to synchronise the converter dq-frame to the network AC voltage reference frame.

As mentioned earlier, LCC-HVDC cannot operate in very low SCCs network, while the VSC-HVDC is still able to. However, this fact does not entail that such operation is without issues. When a VSC is operated in a network with low SCC, the change in AC network voltage, U_L , to a change in injected current is large and has to be compensated in the controller. Model uncertainties are also generally more prominent in systems with low SCC and therefore a controller robust to model variations is needed [24]. Another issue is that the decoupling of active and reactive

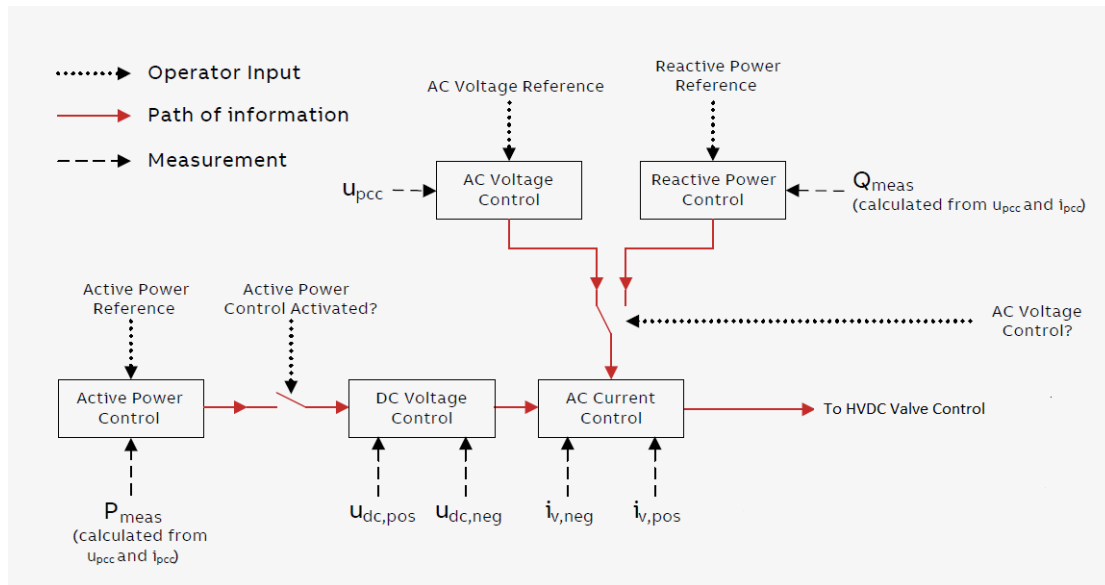


Figure 3.3: The basic control structure of a VSC-HVDC where U_{pcc} and i_{pcc} are the point of common connection voltage and current respectively, which measured in the same point as U_L seen in Figure 3.1 [12]. Photo courtesy of ABB.

power control is not entirely valid when the SCC is low. In networks with high SCC this is not an issue, but when the SCC decreases, the active power control starts to affect the reactive power control and vice versa [24]. This is due to that the off-diagonal elements of the Jacobian transfer matrix increase with lower SCC and thus the dq-frame decoupling is no longer perfect. This requires special care when designing the control loops.

Besides the basic controls displayed in Figure 3.3, high-level controls can be applied to enhance the overall performance. This is done by modifying the active power, reactive power or AC voltage references depending on the desired functionality [26]. For example, emergency power or virtual inertia can be provided by the HVDC converters by measuring the frequency of the network and increasing the active power reference during network disturbances. Power oscillation damping is another example that modifies both the active and the reactive power reference [28].

3.3.2 Limitations in active and reactive power

During operation the control system must take the limitations in active and reactive power of the HVDC converter into account. This yields an operating range of a VSC-HVDC which is limited by three factors [24]. The first one is the maximum current limit set by the valves. This introduces a maximum apparent power limit of the converter. The second limit is the DC over-voltage limit that limits the maximum positive reactive power that can be delivered. To change the delivered reactive power, U_V is changed by adjusting the DC voltage. If the DC voltage maximum

3. HVDC technology

limit is reached, the reactive power becomes limited as well [28]. Thus, the voltage amplitude dictates the reactive power flow [12]. Thirdly, the under-voltage level limits the maximum negative reactive power since the VSC cannot supply active power at too low voltages. A typical operating area for the VSC-HVDC imposed by these three limiting factors can be observed in Figure 3.4. This area is not constant but changes with network conditions [12].

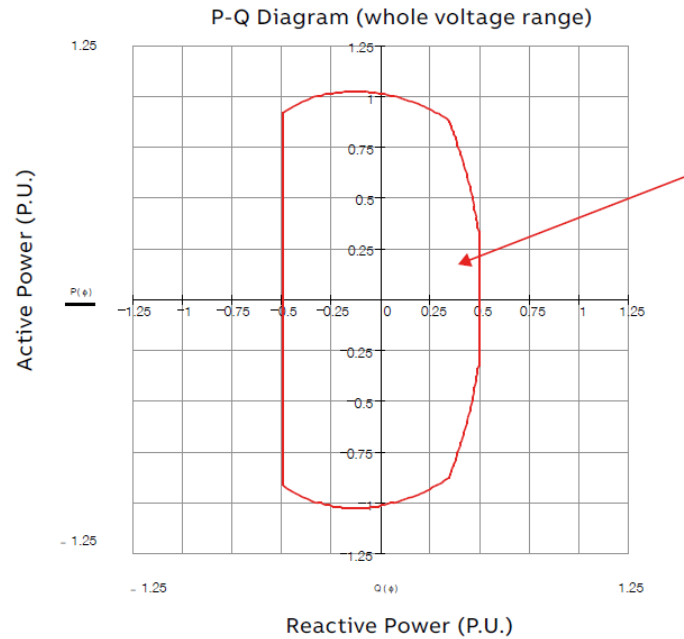


Figure 3.4: A typical operating area of a VSC-HVDC in the PQ-diagram expressed p.u. [12]. Photo courtesy of ABB.

4

Key performance indicators

By thorough literature studies of recent publications by TSOs and research institutes globally, parameters related to short-term frequency and voltage stability have been found and are presented in sections 4.1 and 4.3 respectively. From these parameters, a few KPIs that are deemed the most relevant for classifying frequency and voltage stability in AC grids are selected. The selections of the KPIs are presented in sections 4.2 and 4.4.

The focus of the KPIs is to evaluate the stability of any AC system. However, these parameters are of greater importance in weak AC grids, characterised by the presence of non-synchronous generation and HVDC links. This is due to that the traditional stability measures, also discussed in this chapter, do not fully describe the stability in such grids.

4.1 Frequency stability parameters

The parameters presented in this section are closely bound to the characteristics of the power system frequency during and directly after a large disturbance. In Figure 4.1, the frequency after such a disturbance, where a large amount of generation has been disconnected, is illustrated. In the same figure, some of the parameters presented in this section are shown. The first of these parameters is the gradient of the system frequency slope, commonly referred to as rate of change of frequency (ROCOF). The next parameter is the lowest frequency, the frequency nadir, obtained when the frequency decline is arrested and before the frequency is restored to its initial value. In addition, the time between the disturbance and the frequency nadir is referred to as the time to nadir.

4.1.1 Rate of change of frequency

An important parameter describing the behaviour of the power system frequency after a disturbance is the ROCOF, measured in Hz/s, also denoted df/dt as seen in Figure 4.1. ROCOF is an interesting parameter as it helps to gauge how sensitive

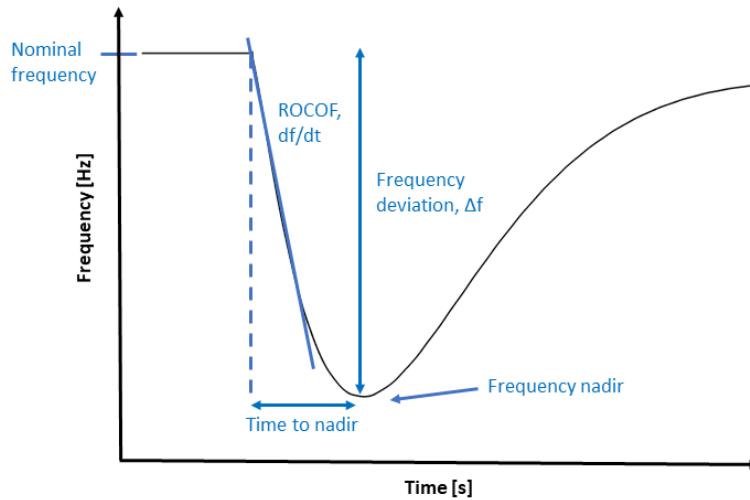


Figure 4.1: Frequency response indicators for the power system frequency after a disturbance.

the system frequency is to disturbances. The ROCOF is highly dependent on the inertial response of the power system, as can be understood from equation (2.10), found in section 2.2.1. Thus, the natural inertia supplied by synchronous generators is the main factor that affects the ROCOF. Another important factor to the ROCOF is the fast active power support that can be provided to the system by the use of power electronic converters, usually as virtual inertia or fast frequency response, discussed in section 4.1.4.1. The fact that the ROCOF takes both virtual inertia and FFR into account is an advantage of this potential KPI, as future networks are projected to contain both of these factors.

4.1.2 Frequency nadir

The frequency nadir, f_{nadir} , is the lowest frequency a system experiences after a contingency event where the demand suddenly exceeds the power supply. For the case of a sudden generator trip, the f_{nadir} is the value of the system frequency where the primary frequency reserves power output have reached the size of the tripped generator [8]. This is an interesting parameter as it is directly comparable to the load shedding frequency limits that are discussed briefly in section 2.2.3. How close the f_{nadir} is to the load shedding limits, and ultimately the under-frequency limit, is a direct measurement of the stability margin of the network, i.e. how close to instability a power system is for a certain fault situation [8].

There are three factors affecting the value of the f_{nadir} after a generator trip: the amount of generation lost, the ROCOF and finally how fast the primary frequency reserve reaches an output equal to the size of the disturbance [8]. The size of the fault determines, along with the inertial response of the system, the ROCOF for a certain fault. How fast the primary frequency reserve outputs power equal to the amount of lost generation determines the time between the disturbance and

the frequency nadir. The combination of how fast the frequency declines and the time when equilibrium of load and generation is restored determines the f_{nadir} . The advantage of f_{nadir} is therefore that it encompasses all factors acting in a system during a frequency excursion.

4.1.3 Time to nadir

The time to nadir, t_{nadir} , is in seconds the time from when the fault occurs to when the f_{nadir} is formed. Its significance is that it displays the time the primary frequency reserve needs to match its output to the lost generation. Thus, a shorter t_{nadir} indicates faster primary frequency reserve, as long as the size of the disturbance is kept constant. However, the rapidness of the primary frequency reserve depends not only on the size of the fault but also on the total available amount of primary frequency reserve and the types of generators that supply the reserve. This makes it complicated to estimate the t_{nadir} .

4.1.4 Inertia

Another frequency stability parameter, indicated in Figure 2.3 in section 2.2.3 discussing the system response to a large disturbance, is the system inertia. The inertia of a power system is expressed with the inertia constant H_{sys} , as presented in section 2.1.2.1. In networks with mainly synchronous generation, the inertia constant can be used to assess the system frequency stability, as H_{sys} is the defining parameter for the ROCOF. However, as the ROCOF does not only depend on the natural inertial response of the system when virtual inertia or FFR is present, the usefulness of H_{sys} as a frequency stability parameter is reduced.

4.1.4.1 Fast frequency response and virtual inertia

Inertial contribution of a synchronous machine is an involuntarily action as the electromechanical connection, which couples the grids electrical frequency to the rotors mechanical rotational speed, dictates that the energy stored up as inertia in the rotor is released when the frequency changes, as shown in section 2.1.2. However, for a non-synchronous generator such as a wind turbine, the rotor is usually decoupled from the grid, as a power electronic converter is used at the interface of the generator. The result is that wind turbines do not involuntarily provide inertial response in a fault situation. Still, a wind turbine could be able to contribute with active power to combat frequency changes if the converter is configured to do so.

The concept of virtual inertia, also known as emulated inertia or synthetic inertia, stems from the fact that inertia is fundamentally only a variation in active power output following a frequency deviation event. A power electronic converter used for

integrating wind power or HVDC into an AC system could therefore also, via its controller, produce the same type of response as a synchronous machine. Still, since the direct electromechanical connection is not present, this has been named *virtual inertia*. There are however two main control strategies for delivering a changed power output, ΔP , during a fault. For the first one, the ΔP is proportional to the ROCOF of the system frequency after the disturbance. For the second one, ΔP is proportional to the frequency deviation, or is applied as a fixed ΔP that is activated when the converter detects a frequency deviation. The ΔP that is proportional to the ROCOF is from now on referred to as virtual inertia, while all other types are called fast frequency response FFR, as defined in [18], [29]. This distinction is made as natural inertia from a synchronous generator is proportional to the ROCOF, and all other types of power increments during a fault traditionally comes from governor control and are thus reserve power.

As discussed in the scope, the focus in this report on the increased power output that can be provided from an HVDC converter during a disturbance is on FFR, and not virtual inertia. This is because FFR is a common method used in literature to simulate the effect of fast acting ΔP from power converters during frequency disturbances [13], [14]. In addition, it can be implemented using a fairly straightforward control strategy.

4.1.5 Primary frequency response

Primary frequency response, not to be confused with primary frequency *reserve* discussed in section 2.2.2, is a measure described in [8] used for assessing the adequacy of the frequency reserves used during primary frequency control in any given power system. In this context, adequacy refers to that the amount of PFR supplied by the generators immediately after a disturbance is sufficient for arresting the f_{nadir} above the highest set point for under-frequency load shedding.

Primary frequency response measures the power delivered from the primary frequency control during a short time frame just before and after the f_{nadir} is reached, both in terms of power output and how fast the primary frequency reserve reacts [8]. In Figure 4.2, a way of measuring the primary frequency response is proposed by [8]. This method measures the primary frequency response at a few predetermined points in time. These values are then compared to values from a benchmark case made for the specific network.

The advantage with the measurement primary frequency response is that it shows how fast the primary frequency reserve acts, which is directly connected to the value of the f_{nadir} . However, it does only encompass one of the parameters that affects the f_{nadir} , and thus, it is not possible to determine the absolute frequency stability of the system from this parameter.

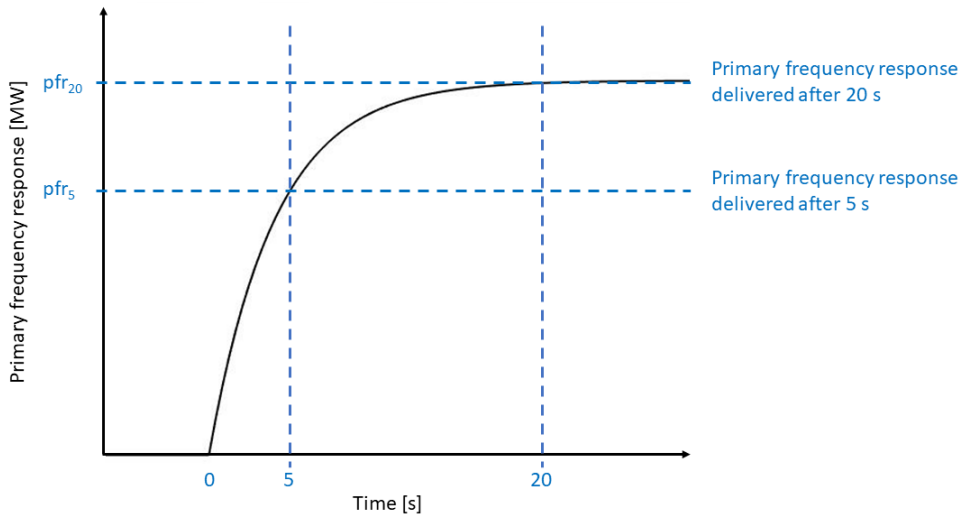


Figure 4.2: An example of primary frequency response measured at 5 and 20 s after initialisation [8].

4.2 Selection of frequency KPIs

To compare the frequency stability parameters defined in section 4.1, simulation studies are performed in MATLAB Simulink. The simulations are executed on a system equivalent model, including only hydro generation, adopted from [13]. In this model, 20% and 40% respectively of the hydro is being replaced with wind power for different case studies. The system inertia, H_{sys} , is 3 s in the base case with 100% hydro generation. For a full model description and additional parameters, see Appendix A.1. In addition to investigating the frequency stability parameters for selection of frequency KPIs, the simulation studies examines the use of FFR for improving the stability of the network. This is made as a part of the investigation on how VSC-HVDC can contribute to the frequency stability of a power system.

In the network, a sudden generation disconnection of 0.1 p.u. of system generation is used to simulate a frequency contingency in all the cases. Further on, in some of the cases, the primary frequency reserve from the hydro generation is modified to investigate the usability of the frequency parameter primary frequency response.

In all cases where FFR is used, the FFR is implemented as a step function with a time span of 10 s and a change in power, ΔP_{FFR} , of 0.05 p.u. of the instantaneous wind generation. These are fairly modest values, chosen as this FFR could be sustained from most turbines in operation with the only assumption that the wind speed is above 6.5 m/s, as firstly presented in [14]. The FFR provided is not unique for wind turbines, but in this simulation case, the limit on the FFR is chosen based on the limit of the minimum rotor speed of the turbines, as discussed in [13], [14].

4.2.1 Simulation studies in MATLAB Simulink

In Figure 4.3, the system frequency behaviour after a disturbance when the system includes wind penetrations of 20% and 40% respectively are presented and compared to the base case with 100% hydro generation. It can be observed that for the case with 20% wind generation, shown as the blue line, the f_{nadir} is lower than for the base case, shown in black. For the case with 40% wind, shown in magenta, the f_{nadir} decreases even further. The ROCOF also gets steeper between these cases, which is reasonable as the inertia of the system is reduced when hydro generation is replaced with wind power. The t_{nadir} changes only slightly, as the response from the primary frequency reserve is faster when the frequency deviation is increased with larger wind penetrations.

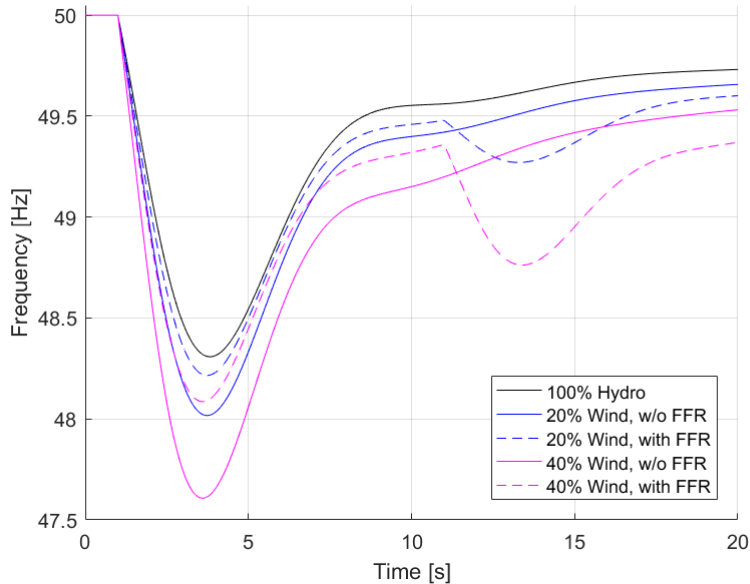


Figure 4.3: System frequency behaviour after a sudden generation disconnection with different amount of wind penetration and with and without FFR.

When FFR is supplied by the wind turbines, as shown by the dashed blue and magenta lines in Figure 4.3, the f_{nadir} increases significantly. The f_{nadir} in the case of 20% wind generation with FFR is close to the f_{nadir} of the base case with 100% hydro. With 40% wind and FFR, the f_{nadir} is higher than for the case with 20% wind without FFR. The ROCOF is also improved when the FFR is in use, but is not better than in the case with 100% hydro generation due to the relatively low FFR power output ΔP_{FFR} . If ΔP_{FFR} is increased to 0.1 p.u. from 0.05 p.u., the result would be a less steep ROCOF and a higher f_{nadir} than in the case with 100% hydro, and thus a larger stability margin than for the base case. This demonstrates the large impact that even a modest amount of FFR provided by power electronic converters has on the frequency stability of a power system.

Figure 4.4 depicts the frequency behaviour when the amount PFR provided by the hydro generation is modified by changing the system equivalent droop, $R_{p,eq}$ and

R_T , seen in Appendix A.1. The black line represents the base case with 100% hydro generation and a 'normal' level of primary frequency reserve, while the continuous blue line represents 20% wind generation with the same level of PFR and the blue dashed line is a case with 20% wind generation and a reduced amount of PFR.

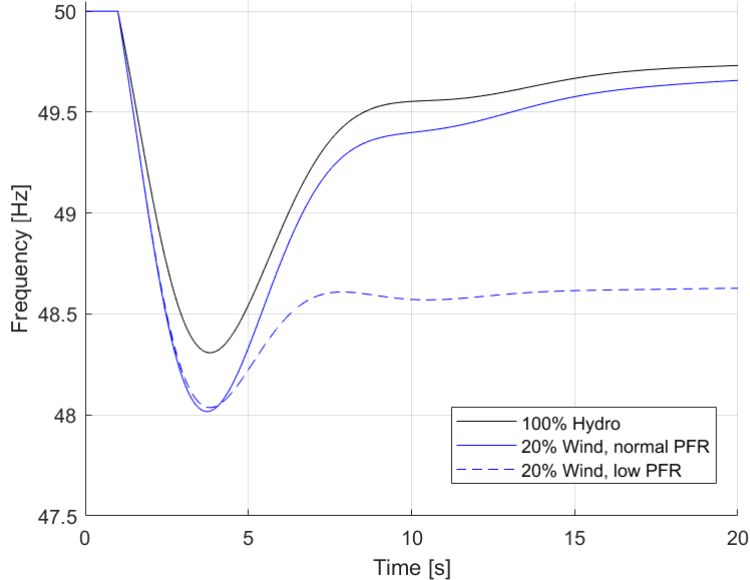


Figure 4.4: System frequency behaviour after a sudden generation disconnection with different amounts of wind power and primary frequency reserve.

From the figure, it can be seen that the amount of PFR marginally affects the f_{nadir} , as both 20% wind cases show very similar nadirs. The PFR is still sufficient in both cases to balance out the lost generation, as if this was not the case, the frequency would continue to decline until the system collapses. These results are reasonable, as the speed at which the PFR is provided does not change significantly when the amount of PFR is reduced. The reason to this is that by changing the droop setting, which dictates the amount of PFR, only the active power reference for the generator changes. As the generator is too slow to follow the change in reference for the first 5 to 10 s, the power output from the generator that contributes to arresting the frequency decline is not affected significantly. However, the settling frequency is affected by the amount of PFR, as the generator has managed to follow the active power reference at this time, several seconds after the f_{nadir} is formed.

The graphs in Figure 4.5 compare the system frequency behaviour when the rapidness of the PFR is adjusted by modifying the equivalent governor time constant, T_g , presented in Appendix A.1. In this figure, 100% hydro is still used as a base case shown in black, and two blue lines with 20% wind power and PFR of different speed are shown. It can be observed that the f_{nadir} is increased by the faster PFR, which is reasonable since the ROCOF is unchanged but the t_{nadir} is decreased due to the faster PFR. However, the response from the hydro governors cannot be made as fast as the FFR supplied by the power electronic converters at the interface of the wind turbines, presented in Figure 4.3. Thus, the stability margin is smaller in this case

compared to when FFR is provided to the system instead of a faster PFR.

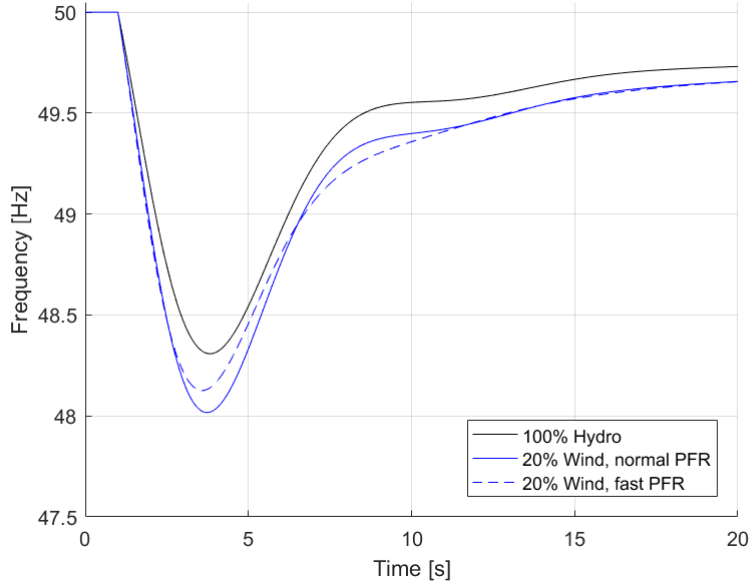


Figure 4.5: System frequency behaviour after a sudden generation disconnection with and without 20% of wind power and different governor time constants for the primary frequency reserve.

In summary, Figure 4.3, 4.4 and 4.5 demonstrate that the most important factor for improving the frequency stability in networks with a large share of non-synchronous generation connected to the system using power electronic converters is to use FFR. Modifying the PFR in magnitude or speed does not seem to have a large impact on the stability margin, and thus, measuring the parameter primary frequency response is not of much interest as it cannot be used to improve the system stability greatly. t_{nadir} does not change significantly with FFR, which makes it unsuitable as a KPI for describing the frequency stability of power systems with a large share of non-synchronous generation. However, it can be observed from the figures that the f_{nadir} as well as the ROCOF changes when the natural inertia of the system is decreased as the wind power penetration is increased, when different amounts of FFR is used and when the PFR is changed.

Finally, as discussed in section 4.1.4, the inertia constant is affected when the wind power penetration is changed. However, when FFR is applied, the inertia constant can no longer be used to assess the system ROCOF accurately, as the inertia of the system remains constant while the ROCOF changes with FFR. Thereby, the inertia constant is insufficient for describing the frequency stability of power systems including non-synchronous generation and HVDC.

4.2.2 Final selection

From the simulation studies in MATLAB Simulink, the first and most important KPI selected for describing the frequency stability of any power system is the frequency nadir. It is chosen based on three characteristics which it possesses. The first one is that the f_{nadir} decreases when the system inertia decreases and increases with the use of FFR. Therefore, the f_{nadir} reflects the changes that are projected to appear when more non-synchronous generation is introduced to power systems globally. Secondly, the f_{nadir} is dependent on three parameters; the ROCOF, speed of the primary frequency reserve and the size of the fault. The interaction of these three parameters defines frequency stability. Lastly, there exists a limit for when instability is reached, which is the under-frequency limit. Thus, one can gauge how close to instability the system is depending the difference between the load shedding limits and the f_{nadir} .

The second frequency KPI to be selected for further research in PSS[®]E is the ROCOF. The most important feature of this measure is that it encompasses the impact of virtual inertia, FFR and natural inertia on a system. Therefore, measuring ROCOF shows more accurately the frequency conserving capabilities of a system compared to estimating an inertia constant for a whole system and applying the swing equation.

This conclusion regarding the frequency KPIs selected in this section has shown to be consistent with results from separate studies of frequency stability parameters presented in [18], [29], [7] and [17].

4.3 Voltage stability parameters

This section defines and selects voltage stability parameters for evaluating the voltage stability of any power system. The limitations of SCC in modern networks including HVDC are discussed and an index for small-disturbance voltage stability, dV/dQ , is defined and presented as a possible KPI for more accurately assessing the power system strength.

4.3.1 Short circuit capacity

Short circuit capacity, presented in section 2.1.4, is a classical voltage stability parameter used for assessing the strength of an AC system, as described in section 1.3.1. The SCC is inversely proportional to the equivalent network impedance during short circuit faults. Thus, the SCC is used as a measure for describing the behaviour of a power system during large disturbances such as short circuit faults. However, in addition to large-disturbance voltage stability, another voltage stability

issue is the small-disturbance, discussed in section 2.3.1. Small-disturbance voltage stability has traditionally not been described with any specific parameter as networks with high SCC usually do not suffer from small-disturbance voltage issues. This is due to that a large value of the SCC implies that there are many sources of reactive power in the system, as the synchronous generators, which provide the SCC, also provide reactive power support to the network. Hence, SCC can be assumed to gauge the overall voltage stability in synchronous generation dominated networks.

4.3.1.1 SCC as a stability parameter in networks with HVDC

When an HVDC station is introduced to a network, the reactive power support is increased and thus the small-disturbance voltage stability of the network is improved. At the same time, the HVDC does not contribute with as much short circuit current as an equivalently sized generator would because of the current limitations of the converter. The SCC and the reactive power support in the network is therefore no longer as strongly correlated to each other as in a network without HVDC. This implicates that it cannot be assumed that a network with a low SCC also has small-disturbance issues. Thus, the SCC measure is no longer sufficient for describing the overall voltage stability of the system when HVDC is present.

Another way of explaining the inadequacy of the SCC parameter when HVDC is present in the system is by using the Thevenin equivalent impedance. The method of calculating SCC based on the Thevenin equivalent during a short circuit fault and assuming that the equivalent impedance of the system is the same in regular operation cannot be applied when HVDC is present. This is the case since the equivalent representation is different for an HVDC in current limitation operation during short circuits and in regular operation. Thus, the equivalent impedance that is reflected by the SCC poorly encompasses the HVDC's effect on the equivalent impedance in regular operation. As a consequence, the network equivalent impedance, which can be used to describe a network strength and voltage stability, cannot be assessed using the SCC alone in networks with HVDC.

4.3.2 dV/dQ

In the late 1980s, A. Hammad at ABB in Zürich presented a new index which he referred to as voltage stability factor (VSF) [30]. The VSF is a measure of the small-disturbance voltage stability and is described as the incremental change in AC voltage at a specific bus that is obtained by a change in load reactive power at the same bus. This is expressed in (4.1),

$$VSF = \left. \frac{\Delta V}{\Delta Q} \right|_P \quad (4.1)$$

where ΔV is the change in voltage in p.u. and ΔQ is the change in reactive power in p.u. on system MVA base, which means that VSF is unitless. P denotes that VSF is valid for a specific load case. In this report, VSF will be referred to as dV/dQ . To understand what dV/dQ indicates in a power system, the classical P-V curve is used. P-V curves based on the basic power system with and without HVDC described in section 4.4 is shown in Figure 4.6. The load case plotted with a dashed line in the P-V curve is 600 MW, and is the same load case as in section 4.4.

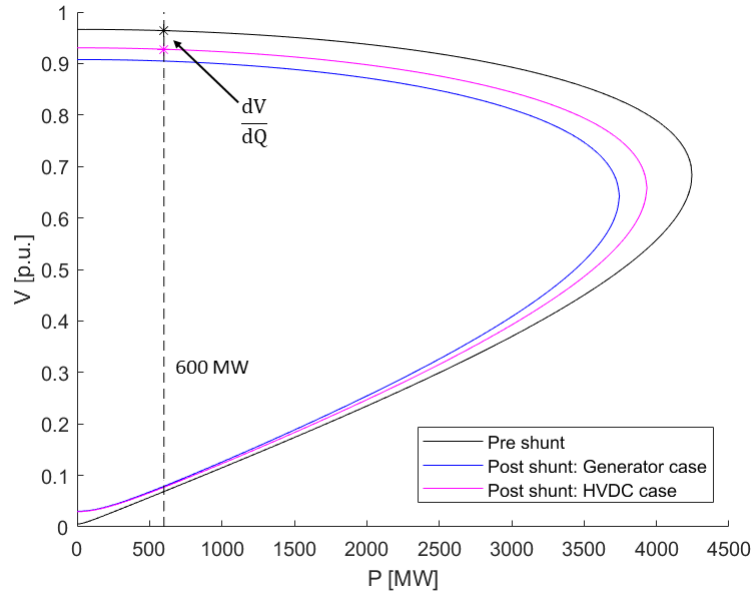


Figure 4.6: P-V curves for the voltage at bus 1 in the basic power system presented in section 4.4. The black graph is before a 200 MVAR shunt reactor is connected to bus 1. The blue and magenta graph are P-V curves after the 200 MVAR shunt reactor has been applied to the system with a generator and an HVDC station respectively.

When dV/dQ is positive, the power system is voltage stable, as a positive injection of Q will increase the voltage. Negative values of dV/dQ indicate that the system is unstable as a positive injection of Q decreases the voltage. This can be observed in the P-V curves shown in Figure 4.6, as a positive value of dV/dQ corresponds to an operating point above the nose-point of the P-V curve, and a negative value to an operating point below the nose-point. More information about how the P-V curve works can be found in section 2.3.1.

Further on, the size of the dV/dQ value indicates how large changes in voltage the system will be exposed to when subjected to disturbances in reactive power [30]. In Figure 4.6, it can be observed that when a shunt reactor of 200 MVAR is connected at the load bus, the P-V curve changes. Comparing the case with only a generator to the case with an HVDC station connected to the simple power system, it can be seen in the figure that the generator case has lower voltage solutions for the same P compared to the HVDC case after the shunt is connected. Thus, the generator case has a larger dV/dQ compared to the HVDC case, as it cannot keep the bus voltage as stiff as the HVDC is able to. Hence, the operating point of the system remains

further away from the stability limit when the dV/dQ is kept low, while the bus voltage is kept at a higher value.

The relation between the dV/dQ and the P-V curve can be used to explain what influences the dV/dQ value. The voltage solutions, $|V|$, of the P-V curve shown in Figure 4.6, can be estimated with

$$|V| = \sqrt{\frac{E^2}{2} - QX \pm \sqrt{\frac{E^4}{4} - X^2P^2 - XE^2Q}}, \quad (4.2)$$

where E is the voltage at the sending bus, Q is the load reactive power, P is the load active power and X is the line impedance [16]. Line resistance is neglected in this formula. It can be observed that the P-V curve, and thereby also the dV/dQ , depend on three factors. Firstly, the ability of the generation sources to maintain the voltage E . Secondly, the network impedance and thus the network topology, described by X , and lastly the active and reactive power consumption of the loads, P and Q . The last one indicates that dV/dQ increases when the system is closer to its maximal power transfer capability. This can be seen in Figure 4.6, as the difference from the black curve to the blue or magenta curve, i.e. dV/dQ , increases with larger values of P .

4.4 Selection of voltage KPIs

To assess the usability of SCC and dV/dQ as KPIs describing the voltage stability of power systems including VSC-HVDC, simulations on a basic power system model are performed in PSS[®]E. This basic power system model has been adjusted for two different cases, where the first case only includes a load, a 110 km transmission line and a single generator with a transformer, as shown in Figure 4.7. In the second case, all components are the same, except that the generator (with transformer) has been replaced by an HVDC model connected to bus 2.

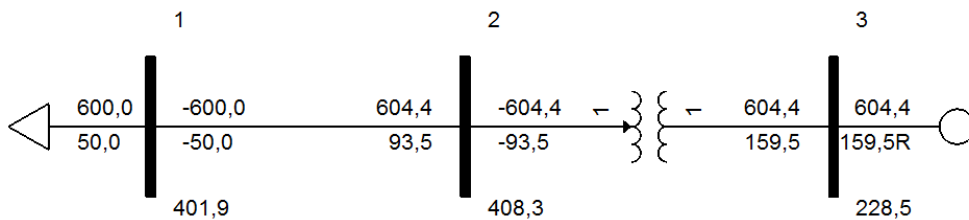


Figure 4.7: A basic power system with a generator and a load. The load flow solution for this system setup in PSS[®]E is shown in the figure, where the voltages are expressed in kV, active power in MW and reactive power in MVar.

In the system shown in the figure, the load has been modelled using an ideal standard model from PSS[®]E. The load, connected to bus 1, demands 600 MW and 50 MVar. The transmission line between bus 1 and bus 2 is identical to the 110 km transmission lines from the Kundur model presented in Table A.1 in Appendix A, and has an impedance of $Z = 0.011 + j0.11$ p.u. with $S_{Base} = 100$ MVA and $V_{Base} = 420$ kV. The generator model is the same as the salient generators used in the Kundur model, presented in Table A.2. The bus voltage at the load buses is 420 kV, while the nominal voltage at the generator bus is 230 kV. In addition, the VSC-HVDC model is rated for 1155 MVA and implemented as described in Appendix A. For more information on the HVDC model and the comparison with an equivalent generator, see section 5.1. For simulations of both cases in PSS[®]E, dV/dQ and SCC have been simulated dynamically using the methods described in Appendix B.

4.4.1 PSS[®]E simulations on a basic power system

In the first case with the generator, the values obtained when simulating dV/dQ and SCC are shown in Table 4.1. In the table, it can be seen that where the system is traditionally considered stronger, i.e. the SCC is higher according to the traditional definition of AC system strength, the dV/dQ is lower. However, when the generator model is replaced by HVDC for the second case, the same table shows that even though the system has lower SCC at each bus, the dV/dQ is improved compared to the previous case. This is an interesting result as it means that the voltages are more stable to small disturbances, even though the SCC traditionally is considered to indicate the opposite. Hence, the correlation between SCC and small-disturbance voltage stability is lost when HVDC is introduced to a power system.

Table 4.1: Measurements of dV/dQ on a 100 MVA base and SCC for the generator and the HVDC case respectively. The load is connected to bus 1, while the generator or HVDC model has been connected to bus 2.

Bus	Generator case		HVDC case	
	dV/dQ [-]	SCC [MVA]	dV/dQ [-]	SCC [MVA]
1	0.030	1922	0.013	1527
2	0.021	2398	0.002	1502

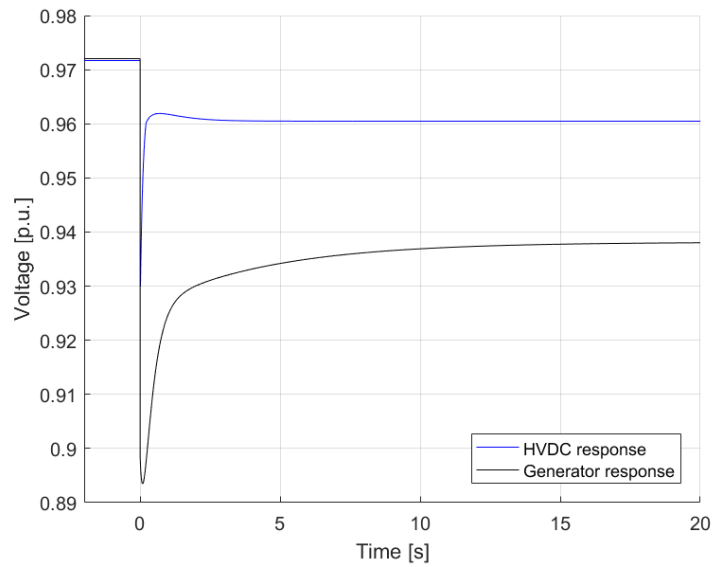
The results shown in Table 4.1 are indicating the same tendency as Figure 4.6, i.e. that the case with HVDC has larger values of the voltage solution compared to the generator case, and thus lower dV/dQ. The explanation to this is that the dV/dQ is dependent on how stiff the sending end voltage E can be held by the source of generation. The HVDC keeps the bus 2 voltage E higher after the 200 MVar shunt reactor is connected to the network than the synchronous generator is able to, and thus the buses in the network have lower dV/dQs. This is illustrated in Figure 4.8a, where the voltage at bus 2 for both cases, with and without HVDC, are plotted when the shunt reactor is connected.

In Figure 4.8b, the voltage at bus 3, where the generator or the HVDC respectively

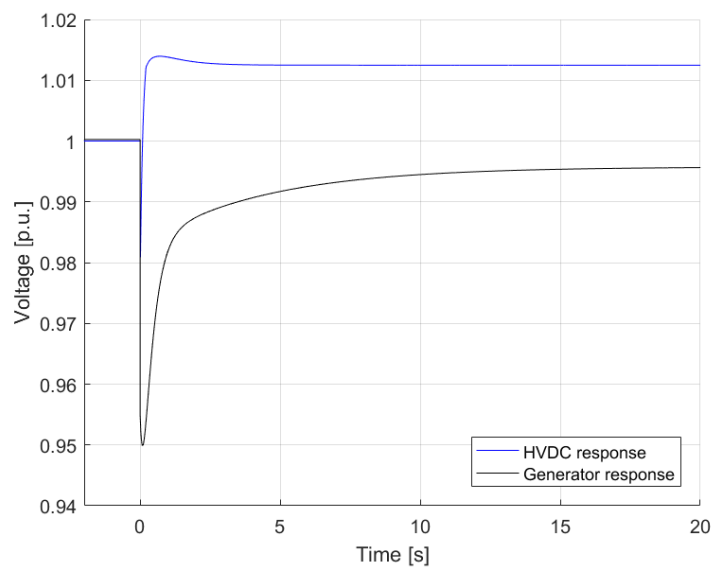
is connected, is shown. The lower dV/dQ value of the HVDC case can be seen more clearly from this figure as the HVDC increases its terminal voltage after the 200 MVar shunt reactor is connected at bus 1. In comparison, the generator case has a reduced terminal voltage because of the lack of an integrating part in the used exciter model "SEXS". However, if a more complex exciter model with an integrating part would have been used, such as the "ESST1A" model used in chapter 6, the voltage would return to its pre-shunt value observed before time $t = 0$ s. The dV/dQ with the "ESST1A" exciter would therefore be improved compared with the "SEXS" exciter, but would still not be as low as in the case with the HVDC.

4.4.2 Final selection

By these simulations it has been shown that the traditional way of characterising system strength based on SCC is not sufficient when HVDC is present in the system. The HVDC clearly adds functionality to the system that cannot be described by SCC as the bus voltages are more stable, i.e. less sensitive to small disturbances, in the case with the HVDC even though the SCC is decreased. dV/dQ appears to be a suitable KPI for describing the small-disturbance voltage stability in a system including HVDC, and is selected for further simulations. Still, SCC holds significance when investigating the large-disturbance voltage stability of a network.



(a) Bus 2 voltage



(b) Bus 3 voltage

Figure 4.8: The voltage at bus 2 (a) and bus 3 (b) for both the generator case (shown as the black graph) and HVDC case (shown as the blue graph) when the 200 MVar shunt reactor is connected at $t = 0$ s.

4. Key performance indicators

5

Simulations on Kundur's network

In a first step of investigating the usability of the frequency and voltage stability KPIs selected in chapter 4, this chapter presents PSS[®]E simulations based on Prabha Kundur's network, described in [15] on p. 813 and used in [31]. This network has been adjusted for two different cases: one case with only generators and a second case where one of the generators has been replaced with an equivalently sized HVDC model. For these two cases, the frequency KPIs are firstly investigated, and then similar evaluations of the voltage KPIs are made. The purpose of the HVDC case is to show how a power network is affected by HVDC and to assess how the KPIs can be used for describing the system strength when including HVDC.

5.1 Introduction to the Kundur network

Prabha Kundur's network is a 4-generators and 11-buses power system. The whole network setup with load flow solution from PSS[®]E for the generator case is shown in Figure 5.1 and discussed more in detail in Appendix A.3. For the case including HVDC, the generator at bus 2 is replaced by an HVDC model, described in Appendix A.2. The point of common connection with the network is bus 6.

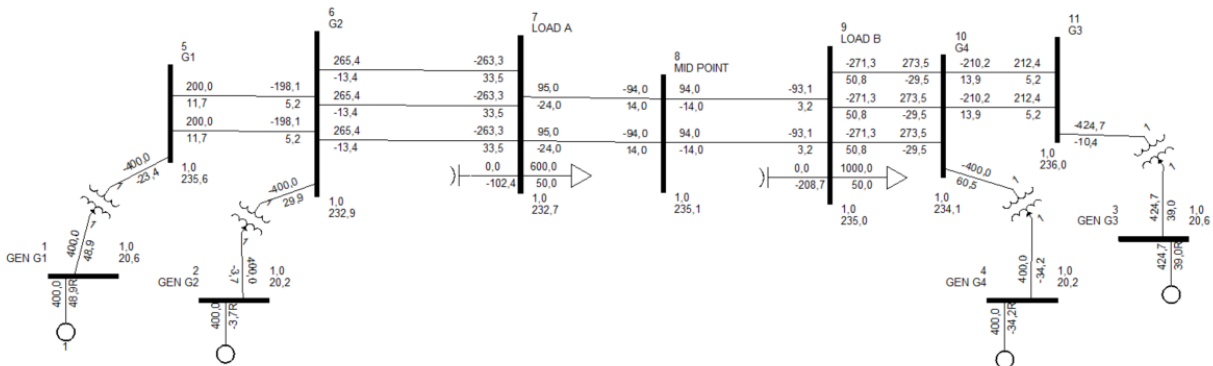


Figure 5.1: Kundur's 4-generator, 11-bus network with load flow solution. Voltages are given in p.u. and kV, active power in MW and reactive power in MVar. A more detailed description of the network is given in Appendix A.3.

The rating of the HVDC converter used for the simulations in the second case is 1155 MVA, as it is a standard rating used by ABB. This can be compared with the rating of the generator connected to bus 2 in the first case, which is 900 MVA. To verify that the HVDC and the generator can be considered equivalent in terms of size, simulations are also made with a 759 MVA HVDC converter, which is another standard rating. When comparing the chosen KPIs, the results are very similar compared to when the 1155 MVA rated HVDC is used. Therefore, the generator and HVDC station are assumed comparable independent on if the 1155 or the 759 MVA HVDC converter is chosen. The results in the following sections are thus results from the simulations with the 1155 MVA rated HVDC converter.

5.2 Evaluation of frequency KPIs

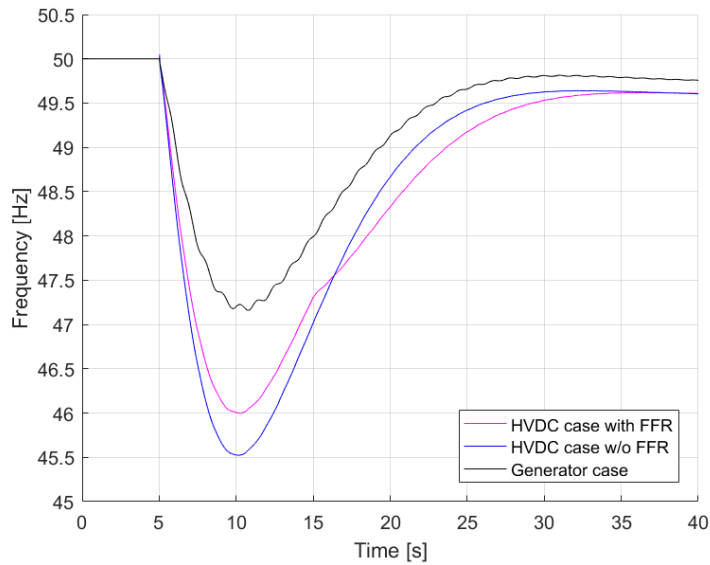
For the frequency simulations in the Kundur network, a third simulation case will be added to the two cases, without and with HVDC, presented in the introduction to this chapter. In the third case, generator 2 is replaced with an HVDC model providing FFR of 40 MW for 10 s. In all three simulation cases, the same disturbance to the system has been applied, which is a disconnection of generator 4 shown in Figure 5.1. Worth noticing is that when generator 4 is tripped, 400 MW of active power generation is disconnected from the system. This is a very large share of the total generation of 1600 MW.

The f_{nadir} and the ROCOF for all the three simulation cases are presented in Table 5.1. It can be seen that the system frequency for the case with only generators is the one with the largest stability margin, as the f_{nadir} is highest in this case. Still, the f_{nadir} is very low and the ROCOF is steep for all of the three cases, as the generator that has been disconnected is very large compared to the total system load.

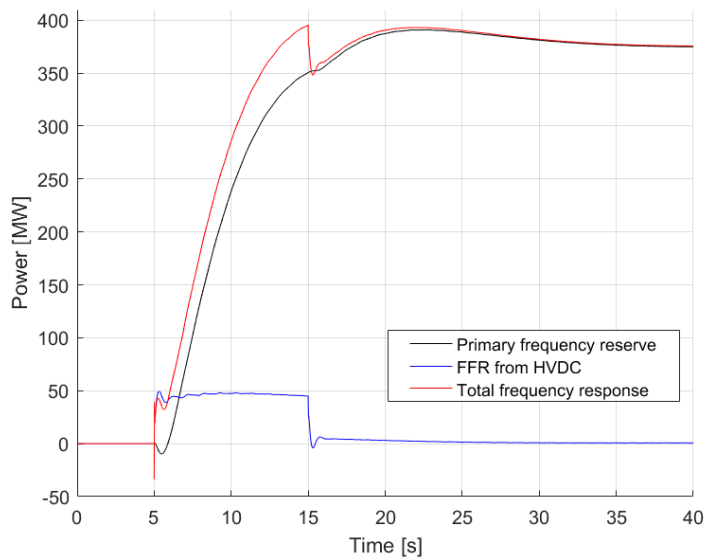
Table 5.1: f_{nadir} and ROCOF for the three frequency simulation cases applied to the Kundur network presented in Appendix A.3.

	f_{nadir} [Hz]	ROCOF [Hz/s]
w/o HVDC	47.2	-0.9
HVDC w/o FFR	45.5	-1.6
HVDC with FFR	46	-1.4

Further on, illustrations of the frequency behaviour for the three simulation cases are shown in Figure 5.2a. It can be seen that in the case with only generators, frequency oscillations occur. These oscillations are due to the inherent oscillations designed into the Kundur network, as the Kundur network originally was used for power oscillations studies [31]. The oscillations are not visible in the other cases, as the HVDC has the ability of reducing frequency oscillations by rapidly adjusting its power output, counteracting changes in power flow. In Figure 5.2b, the PFR from the generators and the FFR provided by the HVDC are plotted for the case with HVDC using FFR, shown as the magenta curve in Figure 5.2a.



(a) The system frequency behaviour when generator 4 is disconnected.



(b) Primary frequency reserve provided by all generators (in black) and FFR provided by the HVDC (in blue) plotted against the total frequency response from all units (in red) for the magenta case shown in Figure 5.2a.

Figure 5.2: Frequency simulations for three cases: a first case with only generators, a second case with HVDC without FFR, and a third case with HVDC using a FFR of 40 MW for 10 s.

From Table 5.1 and Figure 5.2a, it can be seen that the f_{nadir} decreases and the ROCOF increases for the case with HVDC compared to the case without HVDC. This is reasonable as the system inertia is reduced when the generator at bus 2 is replaced with HVDC, and no FFR has been activated to counteract that loss. In the case with HVDC using FFR, the f_{nadir} increases by 0.5 Hz and the ROCOF is

reduced by 0.2 Hz/s compared to the case without FFR. Thus, the relatively small FFR of 40 MW provided by the HVDC station has a large impact on the KPIs such that the system frequency stability, and thereby also the system strength, is improved.

To illustrate the limited use for the inertia constant as a frequency stability parameter, one can compare the inertia constants with and without HVDC for the Kundur network. For the Kundur network with only generators, all generators are synchronous and have the same inertia constant of 3 s, and thus, the system inertia H_{sys} is also 3 s. When the HVDC has replaced generator 2, the estimated system inertia has to be recalculated. By using equation (2.5) found in section 2.1.2.1, the H_{sys} can be calculated to 2.25 s for the case with HVDC. Thus, by comparing the two cases with and without HVDC, the inertia constant can be used to understand that the frequency stability margin will be reduced in the case with HVDC, as the inertia constant is lower. However, if one compares the f_{nadir} between the cases with HVDC with and without FFR, the difference is 0.5 Hz, while the H_{sys} is kept constant. This is a substantial difference in frequency stability that cannot be observed by only estimating the system inertia. Thus, this increase in system strength cannot be measured with the inertia constant, as predicted in section 4.2.1.

Finally, worth to mention is that if virtual inertia instead of FFR is provided by the HVDC converters, a fictive inertia constant H_{vi} can be one of the control parameters to determine the extra active power output, depending on realisation strategy. In such a case, the control parameter H_{vi} can be added to H_{sys} and this equivalent inertia constant is still useful. However, as there is no generally accepted realisation strategy of providing virtual inertia, the approach of using H_{sys} as a stability parameter can only be used in systems with this specific realisation of virtual inertia. If other realisations of virtual inertia or FFR is used, the H_{sys} is still insufficient as a frequency stability parameter.

5.2.1 Summary

By the simulations in the Kundur network, it has been shown that the selected frequency KPIs, f_{nadir} and ROCOF, changes with the loss of inertia when one generator is replaced with HVDC. In addition, they are both improved when FFR is provided by the HVDC converter. This makes these KPIs useful when assessing the system frequency stability in a network with non-synchronous generation and power electronic converters. They have also proved useful when studying the frequency stability margin of a well-known simulation network, Kundur's 4-machine network.

5.3 Evaluation of voltage KPIs

To assess the voltage stability KPIs by simulations on the Kundur network, the case with only generators and the case with generator 2 replaced with HVDC are used in the same way as for the simulation studies of the frequency stability KPIs. To calculate the SCC and the dV/dQ of each bus in the Kundur network, the dynamic methods described in Appendix B are used. This is done because the HVDC model is more accurate in dynamic simulations, and the same calculation method is preferred to be used in both cases for simplifying the comparison. The results from the simulations on the two cases are presented in Table 5.2. Values from bus 1 through 4 are not presented in the table, as those are generator buses and therefore the SCC or dV/dQ will not change significantly between the two cases.

Table 5.2: Measurements of dV/dQ and SCC in the Kundur network for the two cases with and without HVDC respectively. The HVDC model is connected to bus 6 in the HVDC case. Buses in bold are furthest away from generation and are therefore most sensitive to disturbances in the network.

Bus	Generator case		HVDC case	
	dV/dQ [-]	SCC [MVA]	dV/dQ [-]	SCC [MVA]
5	0.012	3936	0.012	3145
6	0.011	4414	0.002	2773
7	0.020	3480	0.011	2567
8	0.040	2130	0.039	2177
9	0.020	3480	0.021	3590
10	0.012	4369	0.013	4473
11	0.012	3898	0.014	3946

For the case with only generators, referred to as the Generator case in Table 5.2, it can be observed that the dV/dQ increases, i.e. the small-disturbance voltage stability is reduced, as the SCC decreases. This can be expected by synchronous generation dominated networks as the SCC is correlated to the impedance of the network, and lower SCC indicates a larger equivalent network impedance and thus to reduced system strength, in accordance with the definition in section 1.3.1. A larger impedance results in that an equal change in MVA_r flow induces a larger voltage deviation compared to a scenario with higher SCC and lower equivalent impedance, and thus the dV/dQ is increased when the SCC decreases. Buses 7, 8 and 9 are located furthest away from generation sources, and lowest SCC along with highest dV/dQ are therefore obtained at those buses.

In the second case, when an HVDC station is connected at bus 6 in the network instead of a generator, the SCC and dV/dQ changes noticeably. As seen in Table 5.2, the SCC is decreased significantly for bus 5, 6 and 7, while the changes are less visible for bus 8, 9, 10 and 11. This is partly due to the fact that the HVDC supplies less SCC than the generator it replaced. However, it also depends on that the SCC a generator provides to the system is dependent on the voltage magnitude

at its terminal during the fault. When a fault occurs far away from the generator, the voltage deviation at the generator terminal is small, as the impedance to the fault is large, and then the generator contributes with less SCC than if the fault would be closer to its terminal. In Table A.1 in Appendix A.3, it can be seen that the lines from 5 to 6 and 10 to 11 are 25 km, from 6 to 7 and 9 to 10 are 10 km and from 7 to 8 and 8 to 9 are 110 km. Therefore, it is reasonable that the SCC will be decreased close to bus 6 for the HVDC case, but not change much at buses further away, since local generation from generator 3 and 4 will still keep the SCC high at buses 9, 10 and 11 but cannot contribute significantly to the SCC of the other buses.

In Table 5.2, it can also be seen that even though the SCC has decreased by 1641 MVA and 1303 MVA for bus 6 and 7 respectively compared to the generator case, the dV/dQ has improved largely. This suggests that the HVDC station increases the dV/dQ greatly even though the SCC has been decreased by a third. Bus 5 has a decreased SCC by 791 MVA for the HVDC case compared to the case without HVDC, while the dV/dQ is the same. For bus 8, the SCC and the dV/dQ are both fairly unchanged if one compares the two cases. This indicates that the HVDC contributes with as much SCC to bus 8 as the generator at bus 2 did in the previous case. In addition, the dV/dQ is also approximately the same.

In general, the generator is expected to deliver more SCC to the network than the equivalent HVDC due to the fundamental characteristics of both technologies. This is a partial truth as can be seen in Table 5.3. In the table, the SCC from generator 2 in the first simulation case without HVDC is shown and compared to the SCC output from the HVDC station in the second case for short circuit faults at buses 6 through 11. It can be observed that the SCC output from the generator is large for buses with short distance to its point of connection at bus 6, but that the output decays greatly with larger distance to the fault, as previously discussed. The HVDC, on the other hand, outputs SCC more evenly. This is due to that the HVDC is controlled to output maximum current during all faults, and thus, as long as the voltage deviation is large enough for the HVDC to detect, the HVDC contributes with about the same SCC to the system irrespective of the distance to the fault.

Table 5.3: SCC output from generator 2 in the first case and from the HVDC station in second case during faults at bus 6 through 11. The point of common connection is at bus 6 for both the generator and the HVDC.

Fault at bus	SCC from the generator [MVA]	SCC from the HVDC [MVA]
6	2281	627.2
7	1681	627.2
8	730.8	920.5
9	503.1	772.7
10	494.1	746.4
11	446.4	584.4

Another interesting note is that the SCC and dV/dQ in the case with HVDC are no longer as strongly correlated as in the case with only generators. For the HVDC case, the dV/dQ is improved at several buses even though the SCC is reduced. This shows that in a system with HVDC the SCC can no longer be used to assess system strength, as the SCC does not correlate strongly with the small-disturbance voltage stability of the network. This can be explained by the fact that the equivalent impedance of the network varies between when the small-disturbance and large-disturbance operation scenarios when the HVDC is connected to the system.

Finally, the droop settings of the generators have been varied in complementary simulations to the studies presented in this section, but no significant change in dV/dQ could be observed compared to the values presented in Table 5.2.

5.3.1 Summary

In summary, the simulations on the Kundur network confirms the conclusion that the SCC cannot be used for describing the overall voltage stability in networks including HVDC, as presented in section 4.4. Instead, dV/dQ can be used to assess the small-disturbance voltage stability of any network, while SCC is kept for describing the large-disturbance voltage stability. By the use of both these measurements, a more complete understanding of voltage stability and system strength can be obtained.

In addition, it has been shown that the HVDC contributes with less SCC to buses close to its terminal than an equivalent synchronous generator, but produces more SCC to buses far away compared to a generator. The HVDC also improves the dV/dQ , and thus the small-disturbance voltage stability, more than an equivalently sized generator.

6

A more realistic simulation case

To investigate the usability of the suggested frequency and voltage stability KPIs for a larger and more realistic system, simulations in PSS[®]E on a power system model based on a North American utility including HVDC are presented in this chapter. To begin with, the characteristics of this network will be presented briefly, moving on to simulation studies on the frequency and voltage KPIs. The ability of the HVDC converters to provide FFR for increasing the frequency stability of this network will also be investigated.

6.1 Introduction to the network

The network used for the more realistic simulation study is a weak AC system located in North America. Every year, load shedding is used to prevent the system from collapse after large disturbances, as the dimensioning fault is large compared to the system load. In addition, the SCC is low. The network is geographically widespread, while delivering power to less than half a million inhabitants. The total system load varies between 600 MW and 1400 MW over the year depending on season. The power generation consists mainly of hydro and some thermal units. A more detailed description of the network and the specific load case used in the PSS[®]E simulations is given in Appendix A.4. An equivalent network diagram for the system is shown in Figure 6.1.

The power system model used in this chapter has been adjusted for two different cases. In the first case, the two HVDC links shown in Figure 6.1 are disconnected, while in the second case, the HVDC links are connected to bus 7. As in the rest of North America, the nominal system frequency is 60 Hz.

6.2 Evaluation of frequency KPIs

To evaluate the selected frequency KPIs for the more realistic network, two different generators have been tripped for the simulations without and with HVDCs. The first

Table 6.1: Measurements of f_{nadir} and ROCOF at bus 5 in the more realistic network without and with HVDC connections.

Case	Outage [MW]	f_{nadir} [Hz]	ROCOF [Hz/s]	Load shedded [MW/MVAr]	Load shedded at time [s]
w/o HVDC	55	58.647	-0.3247	17.08/4.78	8.77
	81.5	58.096	-0.4686	17.08/4.78 39.18/8.82	7.50 10.73
with HVDC	55	58.640	-0.3256	17.12/4.80	8.75
	81.5	58.090	-0.4723	17.12/4.80 39.23/8.84	7.50 10.53

with HVDCs including different amount and time span of FFR are performed to illustrate how this can affect the frequency stability of the network.

In Table 6.2, two scenarios with 25 MW of FFR provided for 10 and 15 s respectively are evaluated, along with one scenario with FFR of 35 MW for 10 s. In PSS[®]E, the FFR has been applied manually at the same time as the generator is tripped, as an HVDC in a practical application is expected to be able to react to a frequency deviation in a very short amount of time (about 50 ms). From the table, it can be seen that when FFR is applied by the HVDCs, the frequency stability of the network is improved significantly compared to the previous cases without FFR. When the 55 MW generator is tripped, no load has to be shedded to arrest the frequency decline in any of the three scenarios with FFR. When tripping the 81.5 MW generator, only one load has to be shed, compared to two loads in the cases without FFR.

Table 6.2: Measurements of f_{nadir} and ROCOF at bus 5 in the more realistic network when HVDCs with FFR are connected to bus 7.

HVDC with FFR	Outage [MW]	f_{nadir} [Hz]	ROCOF [Hz/s]	Load shedded [MW/MVAr]	Load shedded at time [s]
25 MW for 10 s	55	58.939	-0.1748	-	-
	81.5	58.697	-0.3194	17.12/4.80	8.99
25 MW for 15 s	55	59.142	-0.1739	-	-
	81.5	58.697	-0.3192	17.12/4.80	8.99
35 MW for 10 s	55	58.800	-0.1140	-	-
	81.5	58.799	-0.2588	17.12/4.80	8.99

In Figure 6.2, a comparison between the two scenarios with FFR of 25 MW applied for 10 and 15 s respectively for the disconnection of 55 MW is presented. It can be seen that when the FFR is provided for 15 s instead of 10, the f_{nadir} is improved. In addition, the figure shows that the f_{nadir} is the second of two different nadirs for both scenarios, which appears as a response to when the FFR is removed. However, this second nadir could be avoided altogether by ramping down the FFR by the use of a different control strategy.

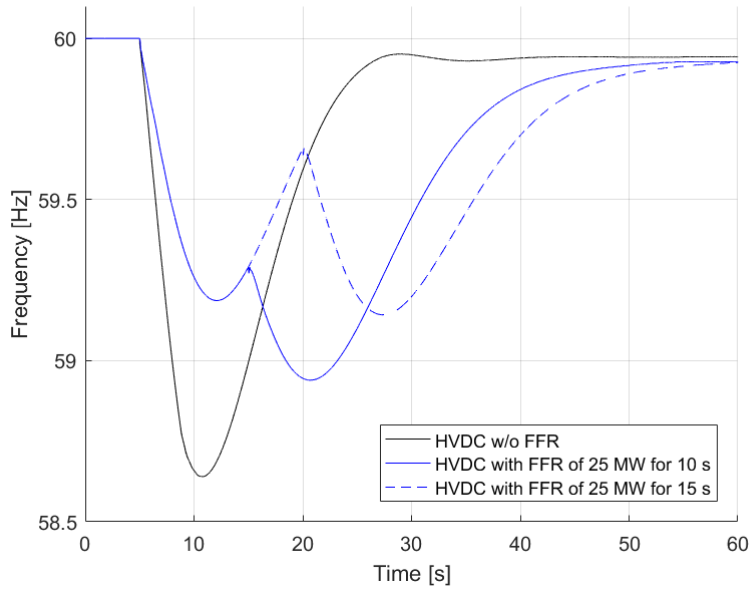


Figure 6.2: The system frequency after the disconnection of the 55 MW generator. The FFR provided is 25 MW for 10 s and 15 s respectively.

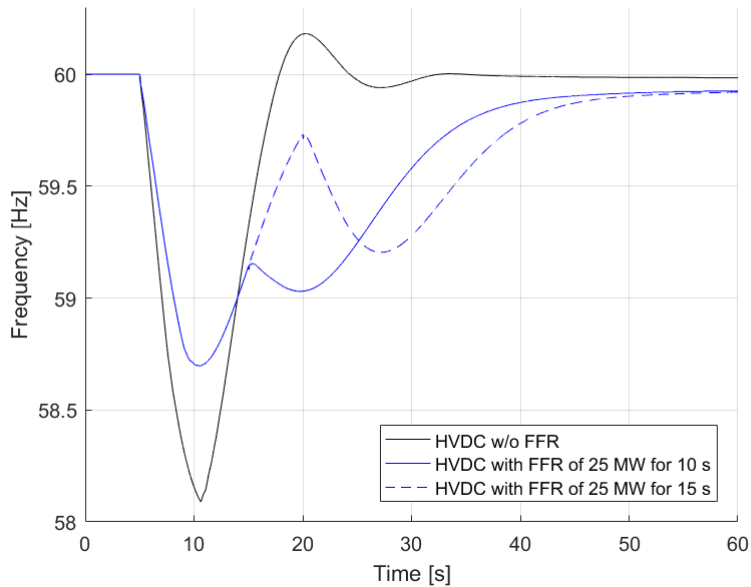


Figure 6.3: System frequency measured at bus 5 after a generator outage of 81.5 MW. The FFR applied for the two blue curves is 25 MW.

When FFR of 25 MW for 10 and 15 s respectively are provided in the case when the disconnected generator is 81.5 MW, the behaviour of the system frequency is shown in Figure 6.3. As the disturbance is considerably larger in this case, the network has to shed one load at 8.99 s after the fault for both scenarios to prevent the frequency from falling too low, even though the FFR is in use. Thus, the 25 MW of FFR is not sufficient if no load is to be shed when the 81.5 MW generator is disconnected.

Further on, the f_{nadir} is found to be the first nadir occurring directly after the load is shedded for these scenarios. The explanation to this is that as the disconnected generator is very large, the disconnection of the generator results in a lower nadir than the removal of 25 MW of FFR.

Next, a comparison between the two scenarios of FFR of 25 MW and 35 MW respectively is given in Figure 6.4 and Figure 6.5. In Figure 6.4, the system frequency for when the 55 MW generator is tripped is plotted, while Figure 6.5 shows the same characteristics but for the disconnection of the 81.5 MW generator. From the both figures, it can be observed that the frequency decline is arrested at a higher frequency after the disturbance when a larger amount of FFR is applied. Thus, the ROCOF is improved significantly. However, as the FFR is only applied for 10 s, the second nadir that comes as a result of the removal of the FFR is significantly lower than the first nadir, and is even lower than the f_{nadir} when the FFR is 25 MW.

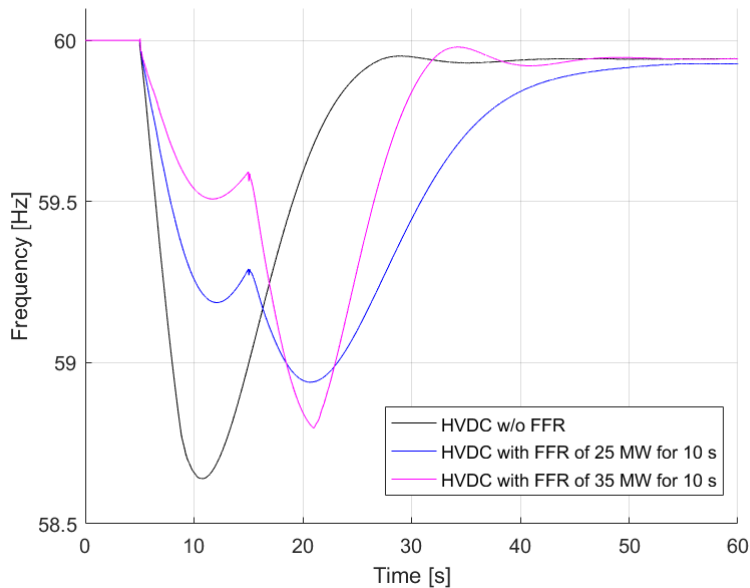


Figure 6.4: System frequency measured at bus 5 after a generator outage of 55 MW. The FFR is 25 MW for the blue curve and 35 MW for the magenta.

In Figure 6.5, it can be seen that when the generator outage is 81.5 MW, the FFR of 35 MW results in an improved f_{nadir} than the FFR of 25 MW, in direct contrast to in Figure 6.4. This can be explained by that as the disturbance is now significantly larger, more FFR is needed to arrest the frequency decline. In Figure 6.5, the second nadir is still lower for the FFR of 35 MW scenario than when the FFR is 25 MW, but it is not having such a large impact on the system frequency as the first nadir caused by the generator disconnection.

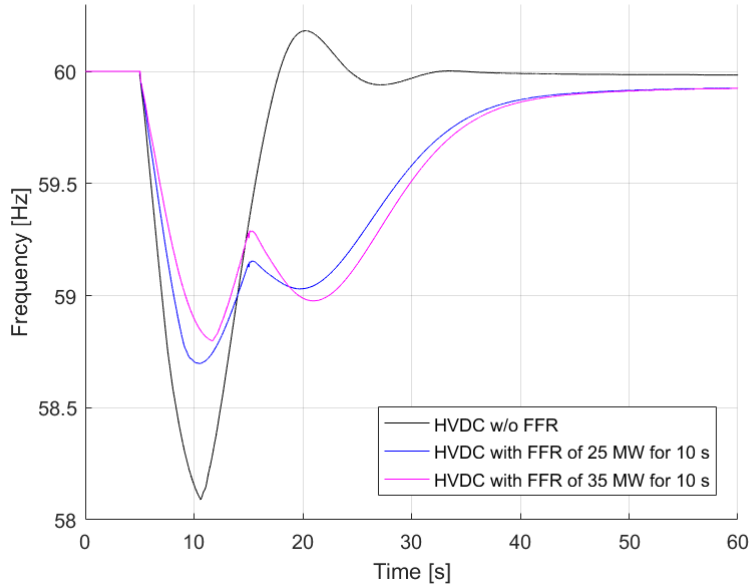


Figure 6.5: System frequency measured at bus 5 after a generator outage of 81.5 MW. The FFR provided by the HVDC is 25 MW in the blue curve and 35 MW in the magenta.

6.2.1 Summary

From the simulations on the system frequency behaviour in the more realistic network, it stands clear that when FFR is provided by the HVDC links, the HVDC converters have the ability of making a significant contribution to the frequency stability. By using FFR, the amount of load that needs to be shedded to arrest the frequency decline after a disturbance is reduced, the ROCOF is less steep and the f_{nadir} is improved. Thus, the frequency can be restored to an acceptable value with a larger safety margin to the under-frequency limit. However, for optimal results, the amount of FFR as well as the time span that the FFR is provided for needs to be coordinated carefully in relation to the size of the disturbance. To avoid the second nadir shown in all the figures, the FFR could also be ramped down. In addition, worth to mention is that in a practical application, the FFR could result in a slower response time for the HVDCs, as this action requires a higher level of control. Finally, the ROCOF and the f_{nadir} have proved to be suitable for describing the frequency stability of a more realistic network including HVDC.

6.3 Evaluation of voltage KPIs

In this section, the selected voltage KPIs are evaluated for the more realistic network using the dynamic simulation methods described in Appendix B.1, in the same way as for the simulations on the Kundur network presented in section 5.3. Thus, dV/dQ

is measured in the network by applying an 100 MVA_r shunt at all the buses in the network, one at the time. Then the SCC is extracted by applying three-phase bus faults at each bus and calculating the fault currents.

From Table 6.3, it can be seen that the voltage sensitivity to changes in Q in the network is lower for all the buses when the HVDC links are in use, compared to when only generators are present in the network. As the two VSC-HVDC links are connected to bus 7, the improvements in dV/dQ are especially clear at this bus and for buses close to bus 7.

Table 6.3: Measurements of dV/dQ on a 100 MVA base and SCC for the more realistic network. The HVDC links are connected to bus 7 in the case with HVDC. Therefore, this bus and the buses closest to bus 7 have been marked with bold letters.

Bus	w/o HVDC		with HVDC	
	dV/dQ [-]	SCC [MVA]	dV/dQ [-]	SCC [MVA]
1	0.0346	1969	0.0344	1970
2	0.0434	1745	0.0431	1736
3	0.0452	1759	0.0447	1757
4	0.0169	3022	0.0161	3023
5	0.0341	1907	0.0296	1998
6	0.0642	1125	0.0566	1224
7	0.0579	1308	0.0046	1592
8	0.0503	1524	0.0361	1686
9	0.0484	1483	0.0286	1688

Further on, it can be seen in the table that the SCC is kept fairly constant for bus 1 to 4 between the two cases. On the other hand, the SCC is improved at the buses close to the point of common connection of the HVDCs, bus 6 to 9, compared to the case without HVDC. The first reason to this is that the distances to the point of connection of the HVDCs are shorter for bus 6 to 9 than for bus 1 to 4. This can also be explained by that in the simulations on this network, in contrast to the simulations on Kundur's network in chapter 5, no generator is removed when the HVDC links are connected. Instead, the HVDCs come into the network as an addition to the generators. Thus, it is clear that HVDC links improves the SCC when added to the network, but not as much as equivalent generators would have.

From the results in Table 6.3, it can be observed that the voltage at bus 7 is kept stiff by the HVDC converters during normal operation as the dV/dQ is low. Compared to the case without HVDC, the dV/dQ at this bus is improved by 92 %. The SCC at bus 7 is also improved, but compared to the case without HVDC, the SCC is only improved by 21.7 %. Thus, it is shown that SCC alone is not a suitable measure for describing the overall voltage stability of a power system when HVDC is present, and that the dV/dQ is useful as a complement for describing a network's sensitivity to small voltage disturbances. This confirms the results seen from the simulations on Kundur's network in section 5.3.

6.3.1 Summary

The simulations on the more realistic network confirms that the parameter dV/dQ is needed to reflect the functionality that HVDC adds to the network, which mainly is related to voltage stability during small perturbations. The HVDC does also contribute with SCC to the network, but not as much as an equivalent generator would. These results corresponds to the conclusions drawn after the simulations on the Kundur network.

7

Discussion

The frequency and voltage stability KPIs defined and selected in this thesis have shown to be suitable for describing the stability of power networks including HVDC. The two frequency KPIs, f_{nadir} and ROCOF, together encompass the impact of classical power system parameters such as inertia provided by synchronous machines, as well as the characteristics of power systems with a large share of non-synchronous generation and power electronic converters, such as virtual inertia and FFR. The two voltage KPIs, dV/dQ and SCC, together describes both the small-disturbance and large-disturbance voltage stability of any power system. Thereby, dV/dQ can also be used as a complement to SCC for describing system strength as defined by the equivalent impedance of the network. These findings are possible to use in a broad context, by grid owners as well as electrification companies such as ABB globally. However, none of the proposed KPIs have any absolute limits that simplifies the TSOs' work in formulating grid codes. This is due to that all power systems are different in size and structure, and thus, what is considered a large disturbance in one network could be a minor event in another. Hence, to formulate suitable requirements for these KPIs, thorough investigations using simulation tools needs to be performed for each specific network.

When evaluating to what extent VSC-HVDC can improve network stability, there is still a lot of work to be done. In the simulations on the Kundur network and the more realistic network, only a few of the existing PSS[®]E models for representing generators have been used, and only one HVDC model. Therefore it is not possible to draw any general conclusions about how much the values of SCC and dV/dQ changes when an HVDC station is connected to an AC system and how the control system of the HVDC affects the system voltages. However, there is no doubt that any HVDC model will change the system dynamics, and that the functionality of the HVDC converters have the ability to improve the system voltage stability. The improvements in frequency stability is however generally applicable, as it only is dependent on the magnitude and coordination of the active power used by the FFR, which any HVDC converter has the ability to provide using a suitable control system. The simple implementation of FFR used in this report can be improved further to shape the frequency response more accurately.

Another model choice that affects the dV/dQ is the exciter models used for the generators. In the Kundur network, the simple exciter model "SEXS" is used. "SEXS"

has a proportional gain but no integrating part in its control system. This affects the dV/dQ and most likely makes the generator contribute to higher dV/dQ s in the network compared to a more complex exciter model with an integrating part. However, in the more realistic case study, an example of an exciter model with integrating part, 'ESST1A', is used. Still, the case with HVDC improves the dV/dQ more compared to the cases with only generators in a similar way as in the Kundur network. Thus, the conclusion that the HVDC improves the dV/dQ more than an equivalent generator still holds even when the exciter model is improved.

On the topic of classifying how an HVDC station and a generator can be considered equivalent, discussed in section 5.1 when replacing generator 2 with an HVDC station in the Kundur network, the criteria used is the MVA rating. However, as these technologies are fundamentally different, it is not realistic that a network owner would consider purchasing a generator or an equally rated HVDC and place them at the same spot in the network. Hence, there could be more efficient ways to make sure that the generator and HVDC comparison is realistic. For the simulations on the more realistic network, on the other hand, the network before and after HVDC is connected to the system is compared while the generator setup is kept constant. This is more often the case for a network owner.

Finally, the societal impact of this thesis is that by using the selected KPIs, safe operation of power systems including a large share of renewable power generation can be ensured. In addition, by using HVDC converters providing FFR, the frequency stability of any power system can be improved. For example, if windpowered HVDC were to replace thermal generation on many locations around Europe, system inertia would decrease significantly. However, in accordance with the results in this thesis, the reduction of inertial response could be counteracted by implementation of frequency dependent HVDC links using FFR. Further on, the HVDC can also improve the voltage stability of a network as it contributes to the SCC and improves the dV/dQ . These conclusions might result in that more HVDC connections can be utilised in networks worldwide, connecting for example wind farms, remote islanded systems or separate synchronous networks. This could facilitate for more energy trading, increasing the social welfare and contribute to well-functioning power markets. Increasing the number of interconnections also enables more intermittent renewable energy generation in all involved networks, as they can support each other with power reserves. This makes it less costly to introduce a larger penetration of renewable energy while securing the system stability. The environmental impact of such an interconnected power system could also be decreased significantly, contributing to reaching climate goals and a more sustainable society.

8

Conclusion and future work

This thesis has shown that the frequency nadir and the ROCOF are suitable KPIs for describing the short-term frequency stability of any power system. Another popular frequency stability parameter, the system inertia, does not encompass the effects of fast frequency response provided by non-synchronous generators and HVDC links, and is thus considered inadequate for describing the strength of a power system with a large penetration of power electronic converters. For describing voltage stability related to small disturbances in any power system, the dV/dQ is proposed in place of the more classical short circuit capacity. The short circuit capacity does not accurately describe the overall voltage stability when HVDC is present in the system. This is due to that the HVDC has the ability of improving the small-disturbance voltage stability significantly while not contributing with as much short circuit capacity as an equivalently sized generator. However, the short circuit capacity is still considered the most valuable KPI for describing voltage stability related to large disturbances in power systems. Thus, the dV/dQ and the short circuit capacity are proposed to be used alongside as measurements of system strength.

Simulation studies in PSS[®]E show that HVDC using fast frequency response can improve the frequency nadir and ROCOF significantly during sudden generator perturbations. Additionally, the voltage control of the HVDC improves the dV/dQ at buses close to the HVDC terminal more than an equivalently rated synchronous generator. Thus, HVDC can contribute significantly to the frequency and small-disturbance voltage stability of a power system.

Future work consists of evaluating the impact of different HVDC models and their control schemes on dV/dQ . In addition, a more thorough investigation of the coordination of fast frequency response with primary frequency reserves is needed. More sophisticated control schemes that output active power proportional to the ROCOF or the frequency deviation could be of interest. More research into correlating the value of dV/dQ to system instability and system strength as well as defining operating limits of dV/dQ for different power systems should also be investigated. Lastly, a redefinition of system strength in a general context to include the behaviour of networks with high penetration of power electronic converters is recommended.

References

- [1] ABB, “Det här är vi - kort om ABB”, 2018. [Online]. Available: <http://new.abb.com/se/om-abb/kort>.
- [2] Svenska Kraftnät, “Systemutvecklingsplan 2018-2027”, 2017. [Online]. Available: <https://www.svk.se/siteassets/om-oss/rapporter/2017/svenska-kraftnats-systemutvecklingsplan-2018-2027.pdf>.
- [3] National Grid, “Future Energy Scenarios”, 2017. [Online]. Available: <http://fes.nationalgrid.com/media/1253/final-fes-2017-updated-interactive-pdf-44-amended.pdf>.
- [4] S. Baldwin, E. DeMeo, J. Reilly, T. Mai, D. Arent, G. Porro, M. Meshek, and D. Sandor, “Renewable Energy Future Study: Executive Study”, Golden, CO, USA, 2012. [Online]. Available: http://www.nrel.gov/analysis/re_futures/.
- [5] US Energy Information Agency, “Annual Energy Outlook 2017: with projections to 2050”, 2017. [Online]. Available: <https://www.eia.gov/aeo>.
- [6] V. J. Schweizer and M. G. Morgan, “Bounding US electricity demand in 2050”, *Technological Forecasting and Social Change*, vol. 105, pp. 215–223, 2016.
- [7] J. O’Sullivan, A. Rogers, D. Flynn, P. Smith, A. Mullane, and M. O’Malley, “Studying the maximum instantaneous non-synchronous generation in an island system—frequency stability challenges in Ireland”, *IEEE Transactions on Power Systems*, vol. 29, no. 6, pp. 2943–2951, 2014.
- [8] J. H. Eto, “Use of frequency response metrics to assess the planning and operating requirements for reliable integration of variable renewable generation”, *Lawrence Berkeley National Laboratory*, 2011. [Online]. Available: <https://www.ferc.gov/industries/electric/indus-act/reliability/frequency%20responsemetrics-report.pdf>.
- [9] E. Ørum, L. Haarla, M. Kuivaniemi, M. Laasonen, A. Jerkø, I. Stenkløv, F. Wik, K. Elkington, R. Eriksson, N. Modig, and P. Schavemaker, “Future system inertia 2”, *ENTSO-E, Brussels, Tech. Rep.*, 2018. [Online]. Available: http://www.statnett.no/Global/Dokumenter/Kraftsystemet/Systemansvar/Nordic%5C%20report,%5C%20Future%5C%20System%5C%20Inertia2_vfinal.pdf.
- [10] “IEEE Guide for Planning DC Links Terminating at AC Locations Having Low Short-Circuit Capacities”, *IEEE Std 1204-1997*, pp. 1–216, 1997. DOI: 10.1109/IEEESTD.1997.85949.

- [11] P. Kundur, J. Paserba, V. Ajjarapu, G. Andersson, A. Bose, C. Canizares, N. Hatziargyriou, D. Hill, A. Stankovic, C. Taylor, T. V. Cutsem, and V. Vittal, “Definition and Classification of Power System Stability”, *IEEE Transactions on Power Systems*, vol. 19, no. 2, pp. 1387–1401, 2004, CIGRE/IEEE Joint Task Force on Stability Terms and Definitions.
- [12] ABB, “Grid systems HVDC: It’s time to connect — technical description of HVDC light® technology”, ABB, Technical Report, 2017. [Online]. Available: <https://new.abb.com/docs/default-source/ewea-doc/hvdc-light.pdf>.
- [13] N. R. Ullah, T. Thiringer, and D. Karlsson, “Temporary primary frequency control support by variable speed wind turbines—potential and applications”, *IEEE Transactions on Power Systems*, vol. 23, no. 2, pp. 601–612, 2008.
- [14] M. Persson, “Frequency response by wind farms in islanded power systems with high wind power penetration”, PhD thesis, Chalmers University of Technology, Sweden, 2015.
- [15] P. Kundur, *Power system stability and control*, 1st ed. British Columbia, USA: McGraw-Hill, 1994, ch. 2, pp. 17–39, ISBN: 0-07-035958-X.
- [16] T. Van Cutsem and C. Vournas, *Voltage stability of electric power systems*, 1st ed. Springer Science & Business Media, 1998, vol. 441, ISBN: 978-0-387-75535-9.
- [17] J. Björnstedt, “Integration of non-synchronous generation - frequency dynamics”, Master’s thesis, Lund University, Sweden, 2012.
- [18] R. Eriksson, N. Modig, and K. Elkington, “Synthetic inertia versus fast frequency response: A definition”, *IET Renewable Power Generation*, 2017.
- [19] P. M. Anderson and A. A. Fouad, *Power system control and stability*, 2nd ed. New York, USA: IEEE Press power engineering series, John Wiley & Sons, 2003, ISBN: 0-471-23862-7.
- [20] C. W. Taylor, *Power system voltage stability*, 1st ed. USA: McGraw-Hill, 1994, ch. 1-2, pp. 13–16, 17–40, ISBN: 0-07-063184-0.
- [21] E. Ørum, M. Kuivaniemi, M. Laasonen, A. I. Bruseth, E. A. Jansson, A. Danell, K. Elkington, and N. Modig, “Future system inertia”, *ENTSO-E, Brussels, Tech. Rep.*, 2015. [Online]. Available: https://docstore.entsoe.eu/Documents/Publications/SOC/Nordic/Nordic_report_Future_System_Inertia.pdf.
- [22] V. Knap, S. K. Chaudhary, D.-I. Stroe, M. Swierczynski, B.-I. Craciun, and R. Teodorescu, “Sizing of an energy storage system for grid inertial response and primary frequency reserve”, *IEEE Transactions on Power Systems*, vol. 31, no. 5, pp. 3447–3456, 2016.
- [23] H. Saadat, *Power system analysis*, 3rd ed. Alexandria, USA: PSA Publishing, 2010, ch. 11, pp. 499–551, ISBN: 978-0-9845438-0-9.
- [24] L. Zhang, “Modeling and control of VSC-HVDC links connected to weak AC systems”, PhD thesis, KTH, Sweden, 2010.
- [25] M. P. Bahrman and B. K. Johnson, “The ABCs of HVDC transmission technologies”, *IEEE power and energy magazine*, vol. 5, no. 2, pp. 32–44, 2007.
- [26] P.-E. Björklund, J. Pan, C. Yue, and K. Srivastava, “A new approach for modelling complex power system components in different simulation tools”,

-
- Indian Journal of Power and River Valley Development*, vol. 61, no. 9, p. 141, 2011.
- [27] L. Zhang, L. Harnefors, and P. Rey, “Power System Reliability and Transfer Capability Improvement by VSC-HVDC (HVDC Light)”, *Security and reliability of electric power systems, CIGRE regional meeting June 18-20*, 2008.
- [28] S. G. Johansson, G. Asplund, E. Jansson, and R. Rudervall, “Power system stability benefits with VSC DC-transmission systems”, in *CIGRE conference*, 2004, pp. 1–8.
- [29] ENTSO-E, “Need for synthetic inertia (SI) for frequency regulation”, *ENTSO-E guidance document for national implementation for network codes on grid connection*, 2018. [Online]. Available: https://consultations.entsoe.eu/system-development/entso-e-connection-codes-implementation-guidance-d-4/user_uploads/6---igd-on-si.pdf.
- [30] A. Hammad and W. Kuhn, “A computation algorithm for assessing voltage stability at AC/DC interconnections”, *IEEE Transactions on Power Systems*, vol. PWRS-1, no. 1, 1986.
- [31] L. Lima, “IEEE PES Task Force on Benchmark Systems for Stability Controls”, *GEN*, vol. 1, no. 1.030, pp. 20–6,
- [32] CIGRE TF 38.02.08, “Long term dynamics, phase II, final report”, CE/SC 38. WG02, Ref. no 102, Tech. Rep., 1995.
- [33] T. Skånøy, “Steady-state and dynamic converter modeling in system analysis”, Norwegian University of Science and Technology, Master Thesis Report, 2007, pp. IX–XI.

A

Simulation models and networks

In this first part of the Appendix, component models and network diagrams used for simulation studies in this thesis report are presented. To begin with, the system equivalent hydro governor model for MATLAB Simulink, originating from [13], is presented. Then the VSC-HVDC model used in all PSS[®]E simulations is described. Further on, the setup and values used when simulating Kundur's network, found in [15] at page 813, are presented. Important to note is that the Kundur network presented here deviates from the cited work by reduction of the loads and fixed shunt capacitors as well as the power set-points of generator 1, 2 and 4 to match the load changes. Lastly, the network diagram for the more realistic network based on a North American utility is presented.

A.1 Hydro governor model in Simulink

The system equivalent hydro governor model along with turbine and load dynamics are presented in Figure A.1. The values of the parameters are: $R_{p,eq} = 0.05$, $T_g = 0.2$ s, $H_{sys} = 3.0$ s, $D = 1.0$, $T_W = 1.0$ s, $R_T = 0.05$ and $T_R = 5$ s. In the figure, $\Delta\omega$ is the change in rotational speed in per unit, and ΔP_L is the change in active load power in per unit [13].

A.2 VSC-HVDC model for PSS[®]E simulations

The implementation of VSC-HVDC in PSS[®]E is done by representing each of the HVDC converters, which all have a base MVA of 1155, with generic generators and connecting them via a transformer to a PV-bus for the power flow analysis. The DC losses are calculated and accounted for as a difference in active power between the two generic generators, with one generator producing negative active power. For the dynamic simulations, a user written model is deployed to the generic generators. The user written model represents the control systems, the dynamics of the converters and the DC transmission [26]. This model includes the control systems discussed in section 3.3.1, along with relevant high-level control functions.

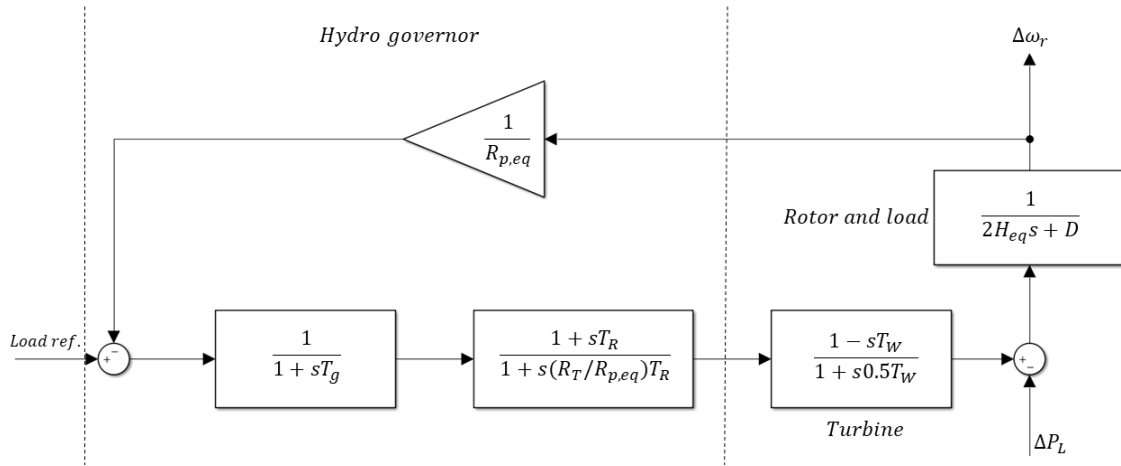


Figure A.1: A MATLAB Simulink hydro governor model with turbine and load dynamics from [13].

A.3 The Kundur network

The Kundur network is a 4-generators and 11-buses system originally used for investigating power oscillations [15]. Figure A.2 displays the network diagram for the Kundur network. As can be seen in the figure, the loads are located at bus 7 and 9, and generators at buses 1 through 4. All generator buses have a base voltage of 20 kV and all the other buses have base voltages of 230 kV. Data for the tie-lines, generators with step-up transformers and loads along with fixed shunt capacitors are presented in Table A.1, A.2 and A.3 respectively. All the step-up transformers have equal properties and are thus only presented once. A general observation is that the network consists of two equal areas, area A to the left of bus 8, and area B to the right of the same bus. Thus, the original network including only generators is symmetric around bus 8. Each one of the two areas has its own generation and load connected by long tie-lines. The exact distances of the lines can be seen in Table A.1. The base frequency of this network has been changed from its original value of 60 Hz to the European standard power system frequency value of 50 Hz.

The power flow solution can be observed in Figure A.2, where the active power flow is in MW and the reactive power flow is in MVar with positive direction out of every bus. The voltage of each bus is displayed in p.u. and kV. In Table A.4, the voltage angles and magnitudes of the power flow solution are displayed with more accuracy.

The dynamic data that has been used for simulations in this report deviates from the data in [15] and [31] since these references lack governor data. Thus, the generator, exciter and governor data used for the simulations in this report comes from the Nordic 32 network presented in [32]. A standard hydro generator with exciter and governor is used as a base for all four generators, with the same dynamic data. The PSS[®]E model names and data are presented in Table A.5.

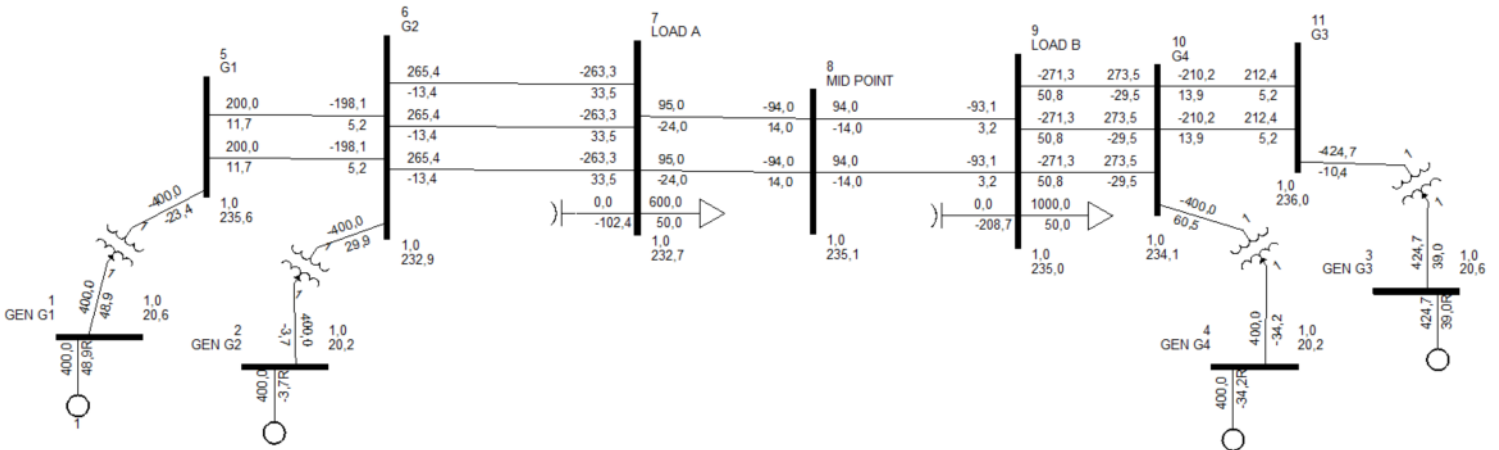


Figure A.2: The Kundur 4-generator and 11-bus network diagram with load flow solution. All bus voltages are expressed in p.u. and kV, active power is presented in MW and reactive power in MVar.

Table A.1: Tie-line data for Kundur's network on a 100 MVA base.

From bus	To bus	ckt ID	Length [km]	R [p.u.]	X [p.u.]	B [p.u.]
5	6	1	25	0.005	0.05	0.021875
5	6	2	25	0.005	0.05	0.021875
6	7	1	10	0.003	0.03	0.005833
6	7	2	10	0.003	0.03	0.005833
6	7	3	10	0.003	0.03	0.005833
7	8	1	110	0.011	0.11	0.192500
7	8	2	110	0.011	0.11	0.192500
8	9	1	110	0.011	0.11	0.192500
8	9	2	110	0.011	0.11	0.192500
9	10	1	10	0.003	0.03	0.005833
9	10	2	10	0.003	0.03	0.005833
9	10	3	10	0.003	0.03	0.005833
10	11	1	25	0.005	0.05	0.021875
10	11	2	25	0.005	0.05	0.021875

Table A.2: Generator (G) and step-up transformer data (T) for Kundur's network on a 900 MVA base (- denotes unapplicable).

Name	Bus	P_{max} [MW]	Q_{max}/Q_{min} [MVar]	R [p.u.]	X [p.u.]	Scheduled Voltage [p.u.]	Tap ratio
T	-	-	-	0	0.15	-	1
G1	1	765	474/-200	0	0.25	1.03	-
G2	1	765	474/-200	0	0.25	1.01	-
G3	1	765	474/-200	0	0.25	1.03	-
G4	1	765	474/-200	0	0.25	1.01	-

Table A.3: Load and fixed shunt capacitor data for Kundur’s network (- denotes unapplicable).

Type	Bus	P [MW]	Q [MVar]
Load	7	600	50
Shunt	7	-	100
Load	9	1000	50
Shunt	9	-	200

Table A.4: Power flow solution with voltage and voltage angle of all buses.

Bus	Bus type	Voltage [p.u.]	Angle [deg]
1	PV	1.0300	10.95
2	PV	1.0100	5.57
3	Swing	1.0300	0.00
4	PV	1.0100	-5.94
5	PQ	1.0241	7.33
6	PQ	1.0128	1.83
7	PQ	1.0119	-2.64
8	PQ	1.0224	-8.53
9	PQ	1.0216	-14.23
10	PQ	1.0178	-9.66
11	PQ	1.0260	-3.84

Table A.5: Dynamic data for used for all generators. Definitions of the models and CONs can be found in PSS[®]E model library, version 33.9 (- denotes not applicable).

Model	CONs											
	J	J+1	J+2	J+3	J+4	J+5	J+6	J+7	J+8	J+9	J+10	J+11
GENSAL	5	0.05	0.1	3	0	1.1	0.7	0.25	0.25	0.15	0.1	0.3
SEXS	0.2	20	50	0.1	0	4	-	-	-	-	-	-
HYGOV	0.04	0.8	5	0.05	0.2	0.1	0.95	0	1	1	0	0

A.4 The more realistic network

The more realistic simulation case is based on an islanded North American utility, which consists of about 650 buses. The original system has basically a few large load and generation centres, complemented with many small loads and generators in sparsely populated areas of the island. The generation is largely hydro, with some addition of thermal generation. For the network model, the original system is reduced to the largest and most important buses of the network, finally represented as the 9-buses network diagram shown in Figure A.3. In the 9-buses diagram, several separate generators on the generation buses have been represented with a

single equivalent generator on each bus to make the diagram more perspicuous. The same method have been applied to the loads. In general, it is a network with long transmission lines, and large distances between load and generation. The length of the transmission lines are presented in Table A.6. The main generation is located at bus 4 and moderate generation is found at bus 1, 5 and 9. The main load centres are located at bus 1, 2 and 9. Thus, as can be observed by the figure, the load centres are far apart and far away from the generation sources. This can be seen in the load flow solution in Figure A.3 as well, where a large part of the generation at bus 4 is transmitted roughly 250 km to the load at bus 1.

In this load case the system does only have a generation of 980.1 MW, which makes it a relatively small system. Furthermore, since it is an island system with two HVDC links at bus 7 as the only connection to another power grid, it is a network with low inertia and SCC. Exact values of SCC for different buses are presented and discussed in depth in section 6.3.

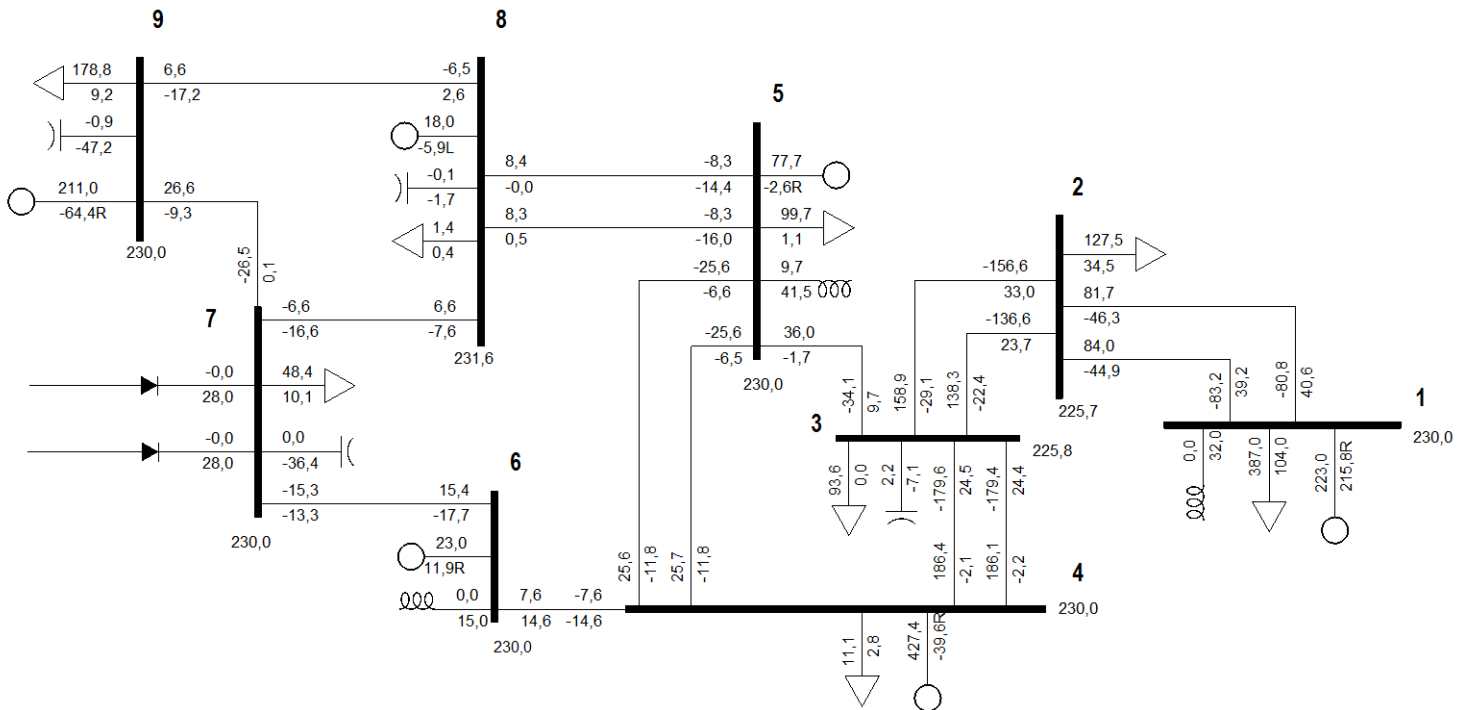


Figure A.3: The network diagram for the more realistic network with load flow solution. Two HVDC stations are connected to 7. The values over the transmission lines are the active power in MW and below are the reactive power in MVar. Each bus has its voltage shown in kV.

In Table A.7, data on the size and dynamic models used for the generators is presented. As stated earlier, the system is hydro dominated and most of the hydro generators contribute to the active power reserves of the system. However, in this load case the reserves are limited as most generators run close to their maximum power output. Finally, the load and shunt data for the simulated load case are presented in Table A.8. The negative G values for the shunts at bus 8 and 9 are results

Table A.6: Transmission line lengths between different buses in the network.

From bus	To bus	ckt ID	Length [km]
1	2	1	65
1	2	2	65
2	3	1	45
2	3	2	52
3	4	1	142
3	4	2	142
3	5	1	120
4	5	1	105
4	5	2	105
4	6	1	126
5	8	1	84
5	8	2	84
6	7	2	180
7	8	1	136
7	9	1	56
8	9	1	85

of the network reductions.

Table A.7: Generator data and dynamic models for the network.

Type	Bus	P_{max} [MW]	Q_{max}/Q_{min} [MVar]	Generator model	Exciter model	Governor model
Thermal	1	340	220/-140	GENROU	SCRX	IEEEG1
Hydro	4	479	310/-360	GENSAL	ESST1A	HYGOV
Hydro	5	80	34/-38	GENSAL	ESAC8B	PIDGOV
Hydro	6	23	19/-20.5	GENSAE	ESST1A	HYGOV
HVDC	7	502	256/-228	ABB model	-	-
Hydro	8	18	5.9/-5.9	GENSAL	None	None
Hydro	9	250	102/-120	GENSAE	BBSEX1	HYGOV

Table A.8: Load and shunt data for the equivalent network in Figure A.3.

Bus	Load data		Shunt data	
	P [MW]	Q [MVar]	G [MW]	B [MVar]
1	387.0	104.0	0	-32.0
2	127.5	34.5	-	-
3	93.6	0	2.3	7.3
4	11.1	2.8	-	-
5	99.7	1.1	9.7	-41.5
6	-	-	0	-15
7	48.4	10.1	0	36.4
8	1.4	0.4	-0.1	1.6
9	178.8	9.2	-0.9	47.2

B

Dynamic measuring methods

As existing load flow based methods for calculating dV/dQ and SCC in PSS[®]E are based on a static models of power networks it is hard to assess the impact of HVDC on the systems in a realistic way. Thus, dynamic simulations, where the the control system in the HVDC can be accurately modelled, are performed instead to achieve realistic values for dV/dQ and SCC when a HVDC station is present.

The dynamic measuring method for calculating dV/dQ and SCC have successfully been verified against load flow measuring methods in non-HVDC cases, which are cases where both methods are valid. The PSS[®]E functions used to calculate comparative values for the dynamic dV/dQ and SCC is Sensitivity analysis and Automatic sequencing fault calculation, respectively.

B.1 Measuring dV/dQ dynamically in PSS[®]E

To measure dV/dQ dynamically, a shunt reactor with a specific MVar value is connected to the bus where the dV/dQ is to be estimated. Then, the dynamic simulation is run until the bus voltage has stabilised, as seen in Figure B.1. The difference between the pre-shunt voltage and the stabilised voltage at the bus is ΔV . Further on, the MVar value of the shunt that is connected at the bus divided by the system MVA base is named ΔQ . From this, dV/dQ is calculated according to

$$dV/dQ = \frac{\Delta V}{\Delta Q} \quad [-]. \quad (\text{B.1})$$

Note that the unit of dV/dQ is per unit voltage divided by per unit reactive power and thus the result is unitless. For the dV/dQ calculations in this report, 100 MVar shunts have been used in all different cases to simplify the calculations as the system base of all networks is 100 MVA.

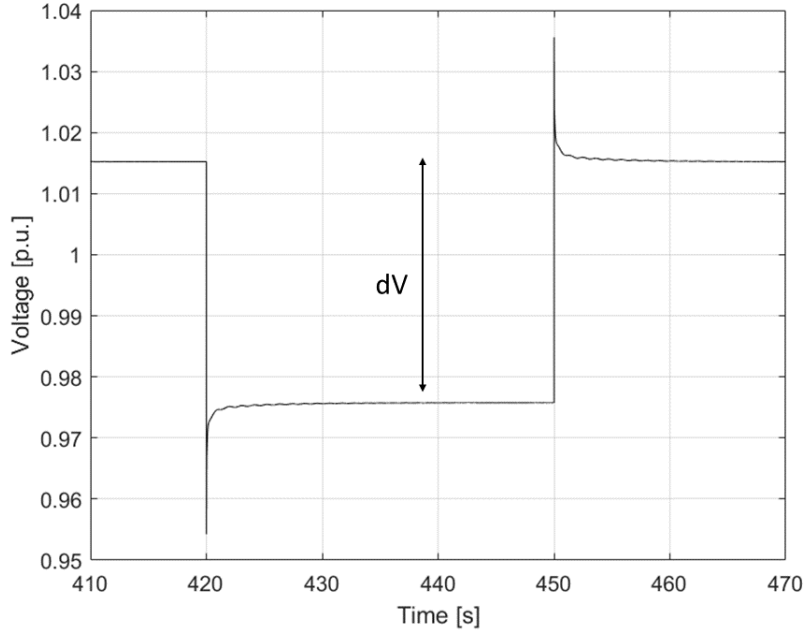


Figure B.1: A visualisation on how dV is measured from a bus voltage when a certain dQ is applied at the bus at 420 s and removed at 450 s.

B.2 Measuring SCC dynamically in PSS[®]E

Measuring SCC using dynamic simulations is no straightforward process as currents cannot be measured directly in PSS[®]E. Therefore, MVA flows and voltage measurements are used to calculate the fault current I_{SC} at every specific bus, as first described in [33].

To estimate SCC dynamically at a specific bus, a three-phase fault with zero fault impedance is applied to the bus for a short amount of time, roughly 0.1-0.2 seconds. Then the short circuit currents from other buses directly connected to the fault bus are estimated by measuring the MVA flows from the lines going into the fault bus along with the voltage at the connected buses. The short circuit current in per unit, $I_{SC,p.u.}$, from each connected line is calculated by

$$I_{SC,p.u.} = \frac{S_{SC,MVA}}{S_n} \times \frac{1}{U_{SC,p.u.}}. \quad (\text{B.2})$$

In this equation, $S_{SC,MVA}$ is the measured MVA flow over the connected line, S_n is the system base in MVA and $U_{SC,p.u.}$ is the per unit voltage of the connected bus. The SCC is then estimated by adding up the $I_{SC,p.u.}$ for all the lines connected to the fault bus and multiplying this sum with the base power, as seen in

$$SCC = S_n \times \sum I_{SC,p.u.}. \quad (\text{B.3})$$

In Figure B.2, the $I_{SC,p.u.}$ has been plotted for a three-phase bus fault at bus 1, in

the basic network shown in Figure 4.7, section 4.4. In this case only one current has to be calculated as only one connection to another bus exists.

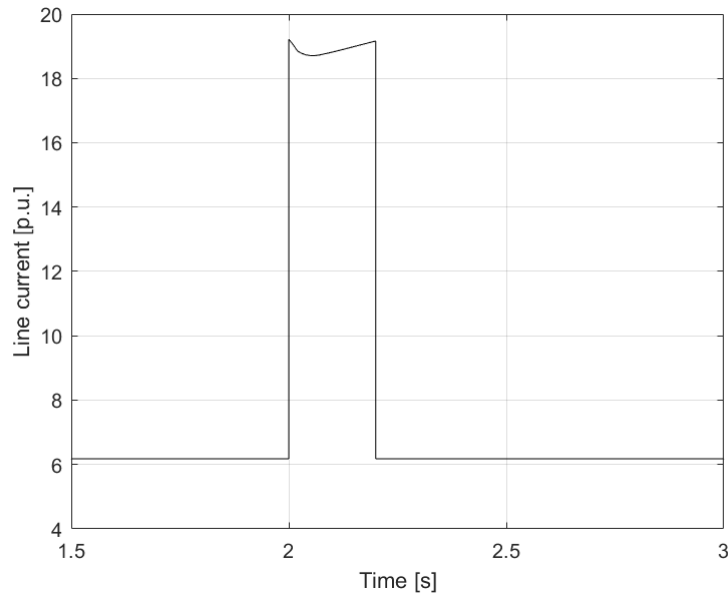


Figure B.2: $I_{SC,p.u.}$ during a short circuit fault in bus 1 for the network described in Figure 4.7, section 4.4. The $I_{SC,p.u.}$ is estimated using the MVA flow from bus 2 to 1 and the voltage in bus 2 according to (B.2).

For this specific example, the MVA flow is measured from bus 2 to 1, and the bus voltage is taken for bus 2. For a more complex network, every connected line's short circuit contribution, $I_{SC,p.u.}$, has to be calculated separately to estimate the SCC of the bus of interest. However, worth to mention is that only the MVA flows from generation buses will be measured, as the load buses do not contribute to the SCC.